Banner appropriate to article type will appear here in typeset article

# Dynamics of turbulent energy and dissipation in channel flow

**Le Yin[1]†, Yongyun Hwang[2] and John Christos Vassilicos[1]**

[1]UMR 9014 - LMFL - Laboratoire de Mécanique des Fluides de Lille - Kampé de Fériet, Univ. Lille, CNRS, ONERA, Arts et Metiers Institute of Technology, Centrale Lille, F-59000 Lille, France

[2]Department of Aeronautics, Imperial College London, South Kensington, London SW7 2AZ, UK

(Received xx; revised xx; accepted xx)

The dynamics of turbulent kinetic energy (TKE), turbulence dissipation rate (TDR) and turbulence production rate (TPR) are explored in fully-developed turbulent channel flow using direct numerical simulations up to $Re_\tau \approx 2000$ with minimal computational box for large-scale structures. Time correlation analysis based on volume-averaged TKE and TDR shows a well-defined average time lag, as in periodic/homogeneous turbulence, which, unlinke periodic/homogeneous turbulence, appears to be Reynolds number dependent. On the basis of a spatio-temporal correlation analysis we show that plane-averaged TKE fluctuations in the near-equilibrium region are transported towards both the core and near-wall regions, and are positively correlated with plane-averaged TDR fluctuations there with combined wall-distance and time lags. In the path towards the core region, the wall-distance lag is very close to the time lag multiplied by the friction velocity. The path towards the near-wall region has a wide spread of time lags which increases with Reynolds number. The spatio-temporal correlation paths both towards the core and towards the wall are reproduced when the reference-plane TKE is conditionally averaged on either ejections or sweeps and are in fact stronger in correlation values in the case of ejections which are better organised than sweeps. While volume-averaged TPR evidently precedes volume-averaged TKE, a more complex picture of non-local space-time correlations between reference-plane TKE and TPR is revealed. A mechanistic model is proposed to elucidate these correlations between TKE and TPR through the interaction between the mean shear and the Reynolds shear stress.

**Key words:** TBC

**MSC Codes** *(Optional)* Please enter your MSC Codes here

## 1. Introduction

Dissipation plays an important role in the dynamics of turbulent flows. In a turbulence that is statistically stationary and homogeneous, the Richardson-Kolmogorov energy cascade

† Email address for correspondence: le.yin@centralelille.fr

Abstract must not spill onto p.2

states that the turbulence kinetic energy (TKE) produced at the large scales is on average carried to smaller scales and eventually dissipated at the smallest scales (Frisch 1995). An equilibrium between the space-time average rate of turbulence generation at the large scales and the space-time average turbulence dissipation at the smallest scales is achieved. However, highly active fluctuations in TKE and TDR appear if such averaging is removed. The feeding and dissipation of turbulence are almost always out of equilibrium. For example, the studies of Goto & Vassilicos (2015, 2016) in forced periodic/homogeneous turbulence showed that the volume-average TDR $\varepsilon_V(t)$ fluctuates in time and correlates heavily with the volume-average TKE $E_V(t)$ with some finite time lag which characterises the average time taken for the turbulence cascade to transport energy from the large energy-containing scales to the small dissipative scales (see Sagaut & Cambon 2008). They also demonstrated that the turbulence dissipation coefficient, defined as $C_\varepsilon(t) \equiv \varepsilon_V/(E_V^{3/2}/L)$ ($L = L(t)$ is the fluctuating integral length scale), is anti-correlated in time with the Taylor-length-based Reynolds number $Re_\lambda(t) \sim E_V/\sqrt{\nu\varepsilon_V}$ ($\nu$ is the kinematic viscosity) without time lag, i.e. $C_\varepsilon(t) \sim (\sqrt{Re_G}/Re_\lambda(t))^n$ where $n \approx 1$ and $Re_G$ denotes a global Reynolds number. $C_\varepsilon$ is a ratio between the rate of energy loss (dissipation) at the small scales and the rate of energy loss at the large scales (by the large-scale eddy turnover). Similarly, $Re_\lambda$ is a ratio of the energy $E_V$ contained mainly in the large scales to the energy $\sqrt{\nu\varepsilon_V}$ contained in the small scales. The strong anti-correlation between $C_\varepsilon$ and $Re_\lambda$ suggests that the turbulence is self-regulating: when the energy at the large scales becomes excessive compared to the energy at the small scales, the large scales tend to lose energy at a higher rate compared to the rate of energy loss at the small scales. This self-regulation appears to be a universal phenomenon present, in one way or another, in a wide range of turbulent flows (see Vassilicos 2015; Vassilicos & Laval 2024)

Recently, Apostolidis *et al.* (2022) investigated this self-regulation (using wall-parallel-plane-average quantities instead of volume-average ones) in the near-equilibrium region of fully developed turbulent channel flow (FD TCF), where the local turbulence energy production roughly balances local turbulence energy dissipation on average (Townsend 1961), and found an exponent $n \approx 3/2$ for the time fluctuations. It was even further demonstrated that the two signals are anti-correlated at all frequencies in this region of FD TCF. However, they did not investigate the possibility of a time lag between TKE and TDR in FD TCF.

The key difference between wall-bounded turbulence and periodic/homogeneous turbulence is the coupling between the boundary conditions and the generation of turbulence. In periodic/homogeneous turbulence, TKE is generated by arbitrary direct forcing of the Navier-Stokes equations, whereas in TCF the no-slip boundary condition at the wall enforces mean shear and momentum transfer between the core flow and the wall thereby leading to production of TKE. Both viscosity and turbulence (through the Reynolds shear stress which is an average of $u'v'$ where $u'$ and $v'$ are streamwise and wall-normal velocity fluctuations respectively) contribute to the momentum transfer and the latter is particularly significant away from the wall where the effect of viscosity is negligible. The contributions of Reynolds shear stress can be classified based on the sign of velocity fluctuations, i.e. the quadrant in $u'$-$v'$ plane (Wallace *et al.* 1972; Willmarth & Lu 1972; Lu & Willmarth 1973). In particular, ejections (Q2 quadrant where $u' < 0$ and $v' > 0$) provide the largest contribution to the Reynolds stress and sweeps (Q4 quadrant where $u' > 0$ and $v' < 0$) provide the second largest contribution to the Reynolds stress throughout a turbulent boundary layer (Lu & Willmarth 1973).

Thanks to the development of numerical simulation and high performance computing, spatio-temporal data of turbulence fields have been made available. In the numerical experiment of Jiménez & Moin (1991), the width of the minimal computational domain

(minimal flow unit) that can sustain TCF was found to be approximately the average spacing of near-wall streaks discovered from the early experiment of Kline *et al.* (1967). By removing the small-scale structures using over-damped large eddy simulation, Hwang & Cossu (2010) identified the largest energy-containing structures in the outer layer that conform with the large- and very-large-scale motions (Kim & Adrian 1999; Guala *et al.* 2006; Hutchins & Marusic 2007*a*).

Energy-containing structures regenerate themselves quasi-periodically and constitute a substantial part of the dynamics of wall-bounded flows (Hamilton *et al.* 1995; Waleffe 1997; Jiménez & Pinelli 1999; Hwang & Bengana 2016). This autonomous cycle is often referred to as the 'self-sustaining process' (SSP). (Doohan *et al.* 2021; Ciola *et al.* 2023). Recent studies on the time evolution of these energy-containing structures suggest that they operate quasi-periodically with a time scale proportional to their size (Lozano-Durán & Jiménez 2014*b*; Hwang & Bengana 2016).

In the present study, we explore the dynamical interplay between TKE, TDR and turbulent production rate (TPR) fluctuations in a relatively small computational box FD TCF at moderately high Reynolds number. Whereas there was no need to study the fluctuations of power input rate in the studies of periodic/homogeneous turbulence of Goto & Vassilicos (2015, 2016) which concentrated on TKE and TDR fluctuations, in FD TCF the TPR fluctuations are part and parcel of small box dynamics and cannot be neglected. We start by exploring the same questions addressed by Goto & Vassilicos (2015, 2016) but now in FD TCF, namely whether TKE and TDR fluctuate in quasi-periodic manner and whether they do so with some time lag relative to each other as in forced periodic/homogeneous turbulence. If so, what are the scalings of this time lag and does it relate to the dynamics of TPR in wall-bounded flows? We finally address the interconnectivity between TPR and TKE dynamics given that TKE needs to be produced before it is cascaded to smaller scales and dissipated.

While such general questions can be asked for any wall-bounded turbulent flow, we limit ourselves to the study of FD TCF using DNS datasets at several different Reynolds numbers with long integration time intervals to obtain well converged statistics and temporal correlations. The size of the computational box is chosen to be the minimal one that can accommodate the largest energy-containing structures in FD TCF as in Hwang & Cossu (2010) without mean statistics such as time-average mean velocity profile and mean energy budgets deviating too far from DNS in larger computational domains (Lozano-Durán & Jiménez 2014*a*; Lee & Moser 2015).

This paper is organised as follows. In §2, we present the numerical setup for our DNS of FD TCF and define our observables in terms of turbulence energetics. In §3, we present our results on the dynamics of TKE and TDR in terms of volume-average temporal correlations, 2-time 1-plane correlations, and 2-time 2-plane correlations of plane-average turbulence energetics. We then focus in §4 on TPR and TKE fluctuations, as well as fluctuations of Reynolds shear stress and mean shear, and introduce a mechanistic model of the fluctuations of mean shear and Reynolds shear stress to account for the space-time lags between TPR and TKE. We summarise our conclusions in §5.

## 2. Numerical methods

We perform DNS of incompressible FD TCF subject to constant mass flux at five different Reynolds numbers: $Re_\tau = 235, 359, 498, 953, 2008$, where $Re_\tau$ is the friction Reynolds number. We denote the streamwise, wall-normal, and spanwise direction by $(x, y, z)$, with the corresponding velocity fields $(u, v, w)$ or $(u_1, u_2, u_3)$. The size of the simulation domain is set to be $L_x = \pi H$, $L_y = 2H$, and $L_z = \pi H/2$, where $H$ is the half channel height. The

| Name | $Re_\tau$ | $N_x \times N_y \times N_z$ | $\Delta x^+$ | $\Delta y^+$ | $\Delta z^+$ | $T_{\text{int}} u_\tau / H$ | $N_t$ |
|---|---|---|---|---|---|---|---|
| R230 | 235 | $96 \times 193 \times 96$ | 11.52 | 0.53 – 4.53 | 5.76 | 183.06 | 3000 |
| R360 | 359 | $144 \times 257 \times 144$ | 11.74 | 0.61 – 5.19 | 5.87 | 172.13 | 3000 |
| R500 | 498 | $192 \times 289 \times 192$ | 12.22 | 0.75 – 6.41 | 6.11 | 164.34 | 3000 |
| R950 | 953 | $384 \times 513 \times 384$ | 11.69 | 0.80 – 6.91 | 5.85 | 151.52 | 3000 |
| R2000 | 2008 | $768 \times 1025 \times 768$ | 12.31 | 0.83 – 7.29 | 6.16 | 92.42 | 2001 |

Table 1: Numerical setup of DNS in FD TCF. $N_x, N_y$ and $N_z$ indicate the numbers of grid points in the streamwise, wall-normal and spanwise directions respectively; $\Delta x^+, \Delta y^+$ and $\Delta z^+$ indicate grid spacings, after de-aliasing, in inner units; $T_{\text{int}}$ denotes the integration time after the initial transient and $N_t$ denotes the number of instantaneous snapshots stored for post-processing.

spanwise extent of the simulation box is comparable to the minimal unit for the self-sustaining process of the largest energy-containing structures as per Hwang & Cossu (2010) and Hwang & Bengana (2016). The size of the simulation domain is deliberately chosen to be small in order to capture the temporal dynamics around the single entity of the large-scale energy-containing structures without significantly modifying the mean statistics (Lozano-Durán & Jiménez 2014*a*). Details of the DNS data set and its naming convention can be found in table 1. We note that integration over a relatively long time interval is required to obtain well-converged statistics 'temporal correlations' in the given computational domain.

The numerical simulation is performed using the Navier-Stokes solver `diablo` (Bewley 2014). The solver uses the Fourier-Galerkin method with a 2/3 de-aliasing rule in the wall-parallel directions $x$ and $z$, and a second-order finite difference method in the wall-normal direction $y$. The temporal discretisation of the solver is based on the fractional-step algorithm by Kim & Moin (1985), with implicit treatment of viscous terms using the Crank–Nicolson scheme and explicit treatment of the remaining terms using a low-storage third-order Runge–Kutta scheme. A snapshot of the velocity field is stored every $1H/U_b$, where $U_b = \frac{1}{V_\Omega} \int_\Omega u \, \mathrm{d}^3\mathbf{x} = 1$ ($\Omega$ is the computatonal domain and $V_\Omega$ its volume) is the bulk streamwise velocity that is kept constant at all time in all DNS. The solver has been verified extensively in previous studies (e.g. Doohan *et al.* 2019).

## 3. Dynamics of TKE and TDR

We first study the dynamics of the TDR and its relation to TKE from the temporal correlation of terms in the TKE budget equation in the wall-normal direction and in time. The velocity field is decomposed as follows: $\boldsymbol{u}(\boldsymbol{x}, t) = (U(y,t), 0, W(y,t)) + \boldsymbol{u}'(\mathbf{x}, t)$ where $(U(y,t), 0, W(y,t)) = \langle \boldsymbol{u}(\boldsymbol{x}, t) \rangle$ and $\langle \cdot \rangle$ denotes averaging over the $x$-$z$ plane. While the Reynolds decomposition has often been used with a mean flow obtained by averaging over time, here we average over wall-parallel planes and extract a time-fluctuating average flow profile, from which the associated Reynolds stresses are derived. Both the average flow and the Reynolds stresses fluctuate in time because of the finite size of the minimal computational domain. We use the notation $\boldsymbol{x} \equiv (x_1, x_2, x_3) \equiv (x, y, z)$ and $(u'_1, u'_2, u'_3) \equiv (u', v', w')$ and two energy budget equations can be considered: one for the kinetic energy $(U^2 + W^2)/2$ of the mean flow which involves neither turbulent transport nor small-scale turbulence dissipation (the dissipation rate in this equation is $\nu[(\frac{dU}{dy})^2 + (\frac{dW}{dy})^2]$ which, unlike TDR, cannot result from a turbulence cascade in $(x, y, z)$ space), and one for the TKE, $\langle u'_i u'_i \rangle / 2$, which does incorporate turbulent transport and cascade-related dissipation dynamics and is obtained by multiplying the governing equation for the fluctuating velocity component $u'_i$ by $u'_i$, summing

Focus on Fluids articles must not exceed this page length

over $i = 1, 2, 3$ and averaging in the $x$-$z$ plane:

$$\frac{\partial}{\partial t}\underbrace{\frac{1}{2}\left\langle u_i' u_i' \right\rangle}_{E(y,t)} = \underbrace{-\left\langle u_i' u_j' \right\rangle \frac{\partial U_i}{\partial x_j}}_{P(y,t)} \underbrace{-\nu\left\langle \frac{\partial u_i'}{\partial x_j}\frac{\partial u_i'}{\partial x_j} \right\rangle}_{\varepsilon(y,t)} + \underbrace{\frac{\mathrm{d}}{\mathrm{d}y}\left\langle -v'(u_i' u_i') \right\rangle}_{T_t(y,t)} + \underbrace{\nu\frac{\mathrm{d}^2}{\mathrm{d}y^2}\frac{1}{2}\left\langle u_i' u_i' \right\rangle}_{T_\nu(y,t)} + \underbrace{\frac{\mathrm{d}}{\mathrm{d}y}\left\langle -v' p' \right\rangle}_{T_p(y,t)}, \tag{3.1}$$

where $\nu$ is the kinematic viscosity of the fluid, $p' \equiv p - \langle p \rangle$ is the fluctuating pressure field and $p$ the full pressure field (the mass density of the fluid is taken to be 1). Note that the three transport terms given in the second line of (3.1) vanish when integrating thoughout the wall-normal direction because of the no-slip boundary condition at the walls. This is not true if we only integrate over the half-channel in the wall-normal direction from the wall to the channel centre where the fluxes are expected to be highly fluctuating in time.

In this paper, we focus on the TKE budget (3.1) because this is the budget directly affected by turbulence cascade (via TDR) and turbulent transport. A top-down approach is employed to study the correlations in FD TCF between TKE $E(y,t)$ and TDR $\varepsilon(y,t)$ on the one hand and TPR $P(y,t)$ and TDR $\varepsilon(y,t)$ on the other. We first explore the dynamics of the overall TKE and TDR by studying the temporal correlation between their volume averages in §3.1, as in the work of Goto & Vassilicos (2015) for periodic/homogeneous turbulence. We volume-average from either wall to the centre line and report the existence of a time lag both between volume-average TKE and volume-average TDR and between volume-average TPR and volume-average TDR. (For all present Reynolds numbers, the frequency spectrum of the volume average $U^2/2$ has one to two orders of magnitude more energy density than the volume average TKE's frequency spectrum at frequencies below $0.5H/u_\tau$ to $H/u_\tau$. The two frequency spectra are however comparable at higher frequencies, and the intensity of time-fluctuations of the volume-average $U^2/2$ is around 1% of its time-average whereas the intensity of time-fluctuations of the volume-average TKE is about 10% of its time-average. $W^2/2$ is very much smaller than TKE with negligible fluctuations.) More detailed dynamical interplay between TKE and TDR is subsequently studied in the wall-normal direction by investigating in §3.2 the temporal-correlation of the plane-average TKE and the plane-average TDR at the same wall-normal location. Overall, the temporal correlation between the two signals is high in the near-wall and in the outer region, but little time lag is observed, suggesting that the time lag observed from the volume-average statistics results from dynamics involving various wall-normal locations. In §3.3, we therefore investigate the temporal correlation between plane-average TKE and plane-average TDR at different wall-normal locations, i.e. $\varepsilon(y,t)$ and $E(y^{\mathrm{ref}},t)$ where $y^{\mathrm{ref}}$ is a reference wall-normal location. A time lag between TKE and TDR is recovered together with a wall-distance lag, revealing the role of inhomogeneity in the spatio-temporal path of energy transfer in FD TCF which is absent in the temporal correlation between plane-average TPR and plane-average TDR. We also report significant temporal anti-correlations in the near-equilibrium region between TKE and TDR with time lag. In §3.4, we investigate the 2-time 2-plane correlations with reference plane taken in the near-wall region and report a Reynolds number dependence of correlation contours. We then average TKE and TDR over regions of ejection and sweeps to further illustrate the link between paths of energy and momentum fluxes in FD TCF in §3.5.

### 3.1. *Volume-average dynamics and correlations*

The volume-average budget equation is obtained by integrating (3.1) from either wall to the centre of the channel:

$$\frac{\partial}{\partial t} E_V = P_V - \varepsilon_V \pm T|_{y=H}, \tag{3.2}$$

where the subscript $\cdot_V$ denotes averaging over the upper or lower half of the computational domain. Without time averaging, the wall-normal transport terms in (3.1) fluctuate in time. The fluxes $\pm T|_{y=H}$ across the centre line are found to be very small compared with the integrated turbulence production $P_V$ and dissipation $\varepsilon_V$.

Figures 1$(a, c, e, g, i)$ present the time signals of volume-average TPR, TKE and TDR for R230, R360, R500, R950, and R2000 (see table 1). While these signals fluctuate heavily around their mean values, TDR seems to have a low frequency content that closely follows TPR and TKE together with some coexisting high frequency content, a behaviour which becomes more apparent with increasing Reynolds number. The time signal of TDR in FD TCF more explicitly displays various times scales than that of TKE, particularly at higher Reynolds numbers, unlike previous observations in homogeneous turbulence (Goto & Vassilicos 2015). This difference might be attributed to the presence of a hierarchy of energy-containing scales or integral length scales in FD TCF.

The time histories of volume-average TKE and volume-average TDR in (3.2) are subsequently studied using a temporal correlation function. For two random signals that fluctuate only in time, say $X(t)$ and $Y(t)$, the temporal correlation function is defined as follows:

$$\rho_{[X,Y]}(\tau) = \frac{\overline{X'(t+\tau)Y'(t)}}{\sqrt{\overline{X'^2(t)}}\,\sqrt{\overline{Y'^2(t)}}}, \tag{3.3}$$

where $X'(t) = X(t) - \overline{X}$ is the fluctuation centred around its mean and $\overline{X}$ is the time average of $X(t)$. The auto-correlation function is recovered for $X(t) = Y(t)$ in which case a maximum value of $\rho_{[X,X]}(\tau) = 1$ is reached for time lag $\tau = 0$.

The temporal correlation functions are presented in figures 1$(b, d, f, h, j)$. Limited by the Reynolds number, R230 and R360 show narrow auto-correlation of volume-average TKE. The auto-correlation functions of volume-average TKE cross zero at roughly $\tau u_\tau/H \simeq \pm 2$ for the higher three Reynolds numbers shown here, suggesting that some aspects, at least, of the dynamics and time scales of large-scale energy-containing structures become approximately independent of Reynolds number when it is high enough (Hwang & Bengana 2016). The auto-correlation functions in figures 1$(b, d, f, h, i)$ show sharper correlation peaks for TDR and TPR than for TKE, presumably caused by the high-frequency content in the dissipation and production signals. The zero crossings of the auto-correlation for TDR and TPR widen as Reynolds number increases, although it remains unclear if this continues with further increasing Reynolds number. Importantly, the peaks of the correlation functions between volume-average TKE and volume-average TDR are roughly at $\tau u_\tau/H \simeq 0.2$ with values of $\rho_{[\varepsilon_V, E_V]}$ between 0.5 and 0.8 (increasing with $Re_\tau$), indicating the presence of an average time lag that is reminiscent of the observations made in forced periodic/homogeneous turbulence by Goto & Vassilicos (2015) (see also figure 3$b$ in Goto & Vassilicos 2016). A similar time lag is also observed between volume-average TPR and volume-average TDR, in fact with even higher values $\rho_{[\varepsilon_V, P_V]}$ (consistently around 0.8 for all five Reynolds numbers) presumably because TPR and TDR are both rates of change of TKE. This time lag is shorter than the typical time scale of the SSP at large scale (Hwang & Bengana 2016). In addition, the correlation functions $\rho_{[\varepsilon_V, E_V]}$ and $\rho_{[\varepsilon_V, P_V]}$ display increasing skewness toward positive time lags at higher Reynolds numbers, spanning the range $\tau u_\tau/H \in [-1, 2]$ for R550 but

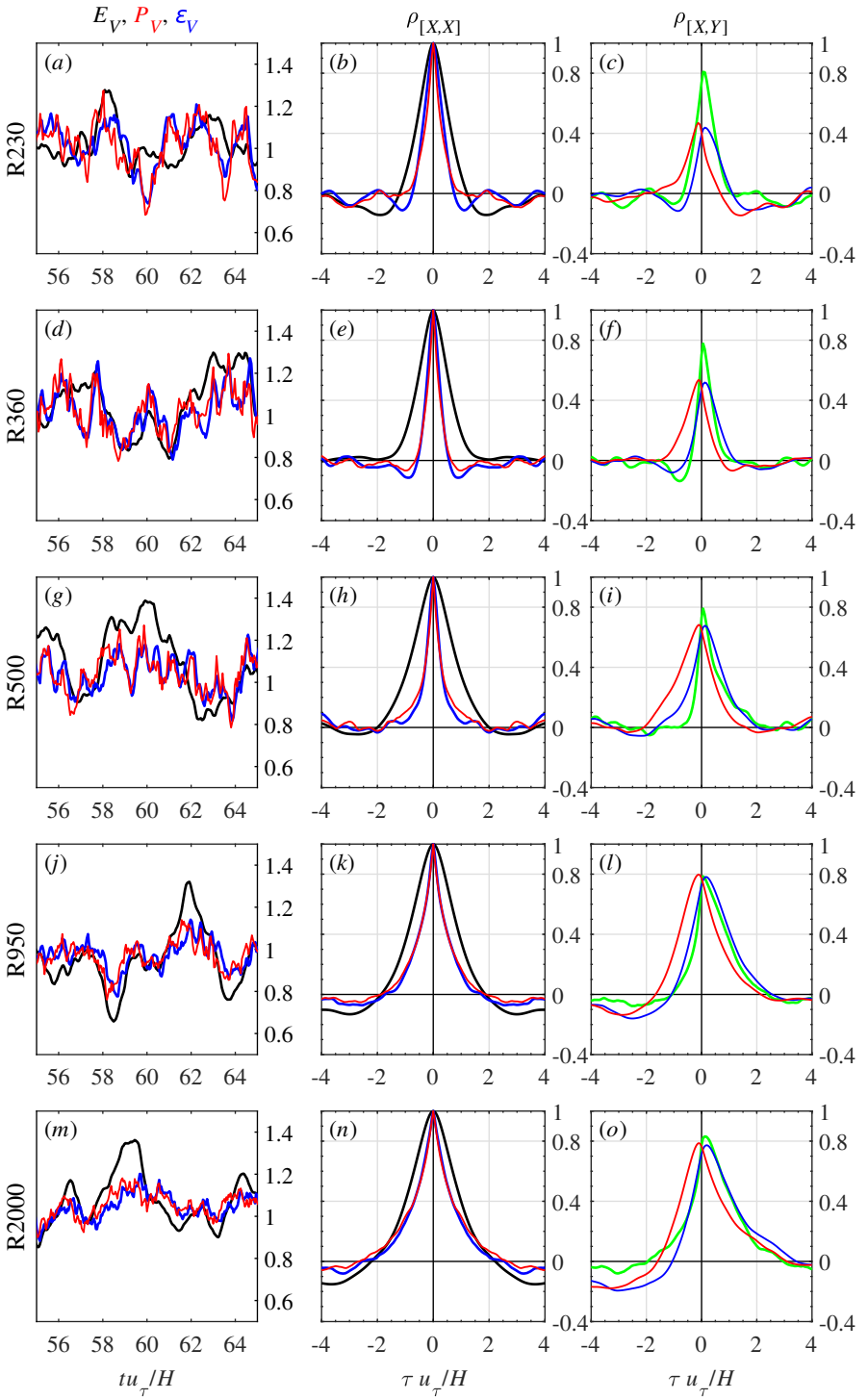



Figure 1: In $(a, d, g, j, m)$, time evolution of volume-average TKE $E_V(t)$ (black lines), volume-average TDR $\varepsilon_V(t)$ (blue lines) and volume-average TPR $P_V(t)$ (red lines), normalised by their time-averaged mean in the lower half channel for five Reynolds numbers. In $(b, e, h, k, n)$, auto-correlations $\rho_{[E_V,E_V]}$ (black lines), $\rho_{[\varepsilon_V,\varepsilon_V]}$ (blue lines) and $\rho_{[P_V,P_V]}$ (red lines). In $(c, f, i, l, o)$, cross-correlations $\rho_{[\varepsilon_V,E_V]}$ (blue lines), $\rho_{[P_V,E_V]}$ (red lines) and $\rho_{[\varepsilon_V,P_V]}$ (green lines).

$\tau u_\tau/H \in [-1, 4]$ for R2000 in the case of $\rho_{[\varepsilon_V, E_V]}$. The skewed correlation function may be interpreted as a 'spread' of time lags (see §3.3).

While we observe a clear positive time lag both between TKE and TDR and between TPR and TDR in FD TCF, it is important to point out that volume-averaging obscures the dynamics associated with inhomogeneity in the interactions between TKE and dissipation. The observed dynamical interplay between TKE and TDR cannot be the same as that found in periodic/homogeneous turbulence (Goto & Vassilicos 2015). We address the impact of vertical inhomogeneity on the interplay between TKE and TDR in the remainder of this section 3 and the interplay between TKE and TPR in section 4.

### 3.2. *2-time 1-plane correlations*

The neglect of inhomogeneity, due to volume averaging, needs to be restored for the detailed picture of the full temporal dynamics between TKE and TDR. We therefore now investigate, as in §3.1, the correlations between time signals of plane-average TKE and plane-average turbulence dissipation rate at different wall-normal locations. In figure 2, we plot time signals of the plane-average TKE and TDR normalised by their plane- and time-average mean values at three locations: the near-wall region at the edge of the viscous sublayer ($y^+ = 10$), the near-equilibrium region where production roughly balances dissipation ($y/H = 0.3$) and the core region ($y/H = 0.8$).

In the near-wall region ($y^+ = 10$ in figure 2 but similar observations hold for $y^+ \leqslant 100$), TKE and turbulence dissipation fluctuate almost concurrently. This is not surprising as there is little separation between the energy-containing scale and dissipative scale in the near-wall region. As the Reynolds number increases (from top to bottom in figure 2), the low frequency signal appears more pronounced. The near-wall time scale becomes shorter and shorter compared to $H/u_\tau$ (used to normalize time in figure 2) as Reynolds number increases. It is interesting to observe that, even so, the TKE and TDR fluctuate almost concurrently even at the highest Reynolds numbers considered here (see figures 2$j, m$). This suggests that the near-wall energy-containing structures (potentially part of large-scale structures extending from the near-equilibrium and outer layers) are directly related to dissipation in the near-wall region.

At $y/H = 0.3$ (figures 2$b, e, h, k, n$), the time signals of plane-average TKE and plane-average TDR do not appear to be well correlated with each other as $Re_\tau$ increases. The same holds true for any $y/H$ between 0.2 and 0.4. Note that this is the region where the large-scale structures are very energetic (Hoyas & Jiménez 2006).

In the core region at $y/H = 0.8$ (though similar observations can be made for $y/H = 0.5$ to 1), TPR is known to be very small due to diminishing mean shear and Reynolds shear stress near the channel centre. The dynamics of turbulence energetics are therefore dominated by turbulence transport and dissipation. The plane-average TKE and the plane-average TDR appear highly correlated instantaneously at the same plane, as shown in figures 2$(c, f, i, l, o)$ for all the Reynolds numbers considered here. As can be seen in the following figure 3, there is no time lag in these correlations and there is therefore no cascade directly linking plane-average TKE and plane-average TDR in the core region.

Similar to the correlation function defined for volume-average variables in time in §3.1, one can define a temporal correlation function for signals in time that depends on the wall-normal location in FD TCF. Figure 3 plots the contours of 2-time 1-plane correlation functions between plane-average TKE and TDR, defined as

$$\rho_{[\varepsilon,E]}(\tau, y) = \frac{\overline{\varepsilon'(t+\tau, y)E'(t, y)}}{\sqrt{\overline{\varepsilon'^2(t, y)}}\sqrt{\overline{E'^2(t, y)}}}, \tag{3.4}$$

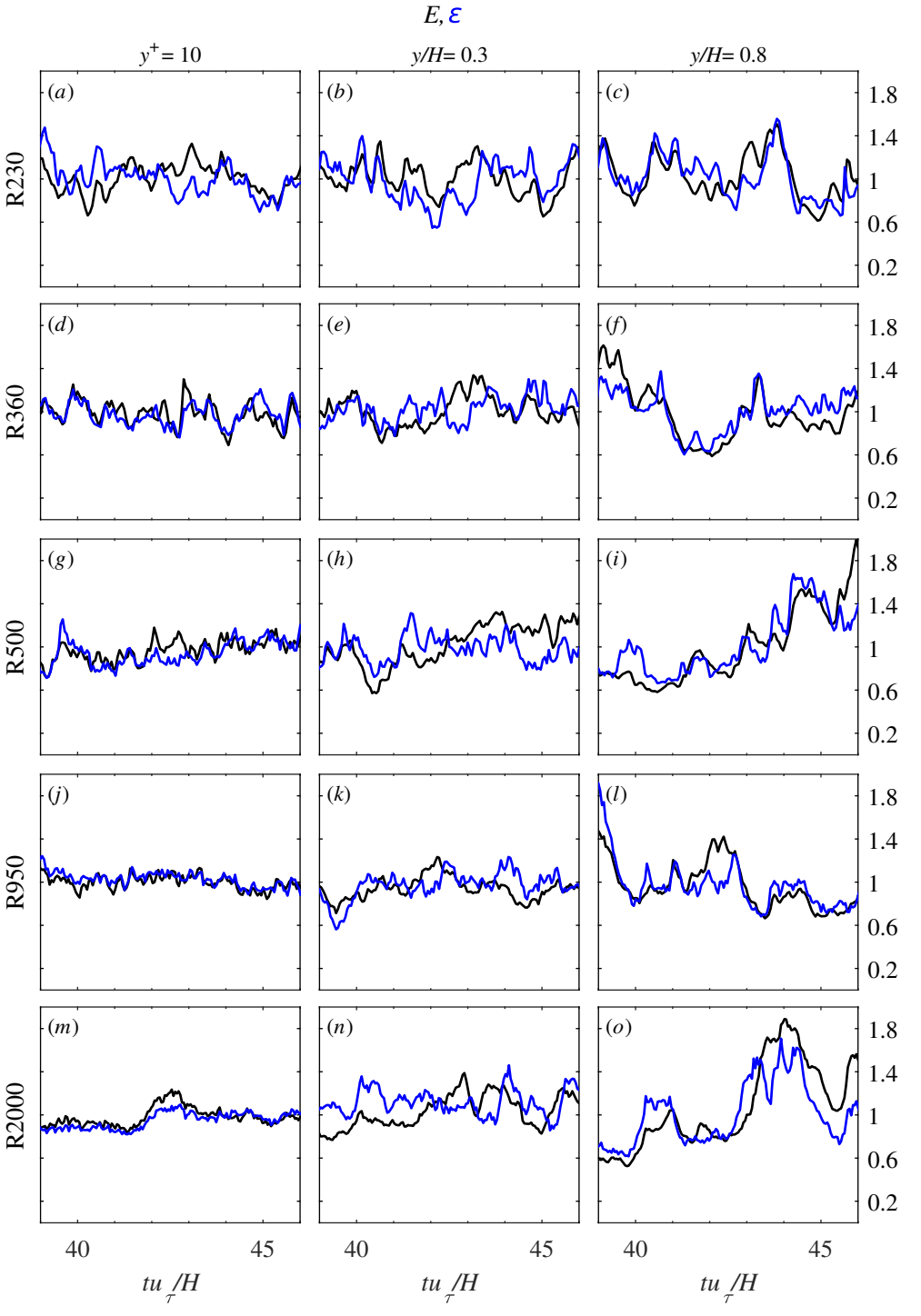



Figure 2: Time evolution of plane-average TKE $E(y,t)$ (black lines) and plane-average TDR $\varepsilon(y,t)$ (blue lines), normalised by their plane- and time-averaged mean in the lower half channel for five Reynolds numbers at three wall-normal locations $(a,d,g,j,m)$ $y^+ = 10$, $(b,e,h,k,n)$ $y/H = 0.3$, and $(c,f,i,l,o)$ $y/H = 0.8$.

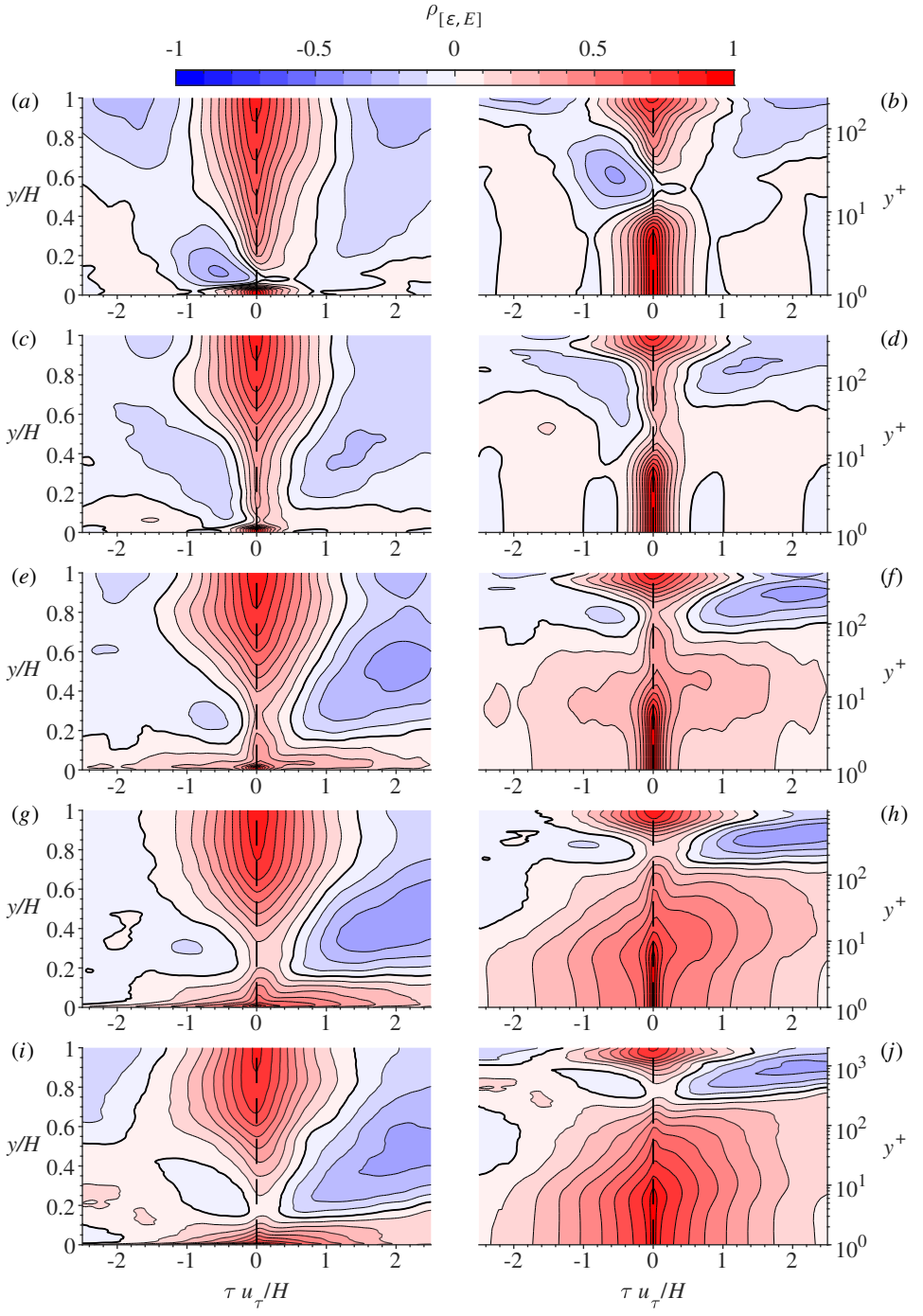



Figure 3: 2-time 1-plane correlation function contours $\rho_{[\varepsilon,E]}$ versus distance from the wall in outer unit $y/H$ with linear axis $(a, c, e)$ or inner unit $y^+$ with log axis $(b, d, f)$ and versus time lag $\tau u_\tau/H$. $(a, b)$ R230, $(c, d)$ R360, $(e, f)$ R500, $(g, h)$ R950, $(i, j)$ R2000. Vertical dashed lines indicate the position of maximum positive correlation as a function of $y$, showing that it coincides with the vertical $\tau = 0$ line.

Rapids articles must not exceed this page length

where $\tau$ is a time difference. From the correlation contours in figure 3, high positive correlations between TDR and TKE in the near-wall region and the core region with zero time lag are observed, as expected from figure 2. The positive correlations in the near-wall region are concentrated in a narrow time window for small Reynolds numbers which widens as Reynolds number increases, reflecting the volume averaged correlation observation in figures 1($b, d, f, h, j$). It may be that, as $Re_\tau$ increases, increasingly energetic structures above the near-wall region influence the near wall region with fluctuations of increasing length and time scales causing positive correlations with an increasing range of time lags in the near wall region. In the near-equilibrium region, the correlation contour shows negative values (anti-correlation) between TDR and TKE with positive time lag, i.e. an increase/decrease in local TKE precedes a decrease/increase in local TDR. Finally, TKE and TDR are strongly correlated throughout the core with both positive and negative time lags $\tau$ in the range $\tau u_\tau/H \in [-1, 1]$ nearly independent of Reynolds number.

In both the near-wall and core regions, the location of the maximum correlation in terms of time lag is always clearly at $\tau = 0$. In the near-equilibrium region it is also near $\tau = 0$ though less rigorously at $\tau = 0$ because of low correlation values there. These zero time lag results have been previously reported for FD TCF (see figures 5$g$, $h$ of Apostolidis *et al.* 2022) using data obtained in a computational domain that is double the size of the present simulations in the streamwise and spanwise directions in terms of multiples of $H$ (Lozano-Durán & Jiménez 2014*a*). In the near-wall region, high instantaneous correlations between TKE and TDR (neither time lag nor lead) are expected, since there is no scale separation there. The high instantaneous correlations in the core region (neither time lag nor lead) suggest that high/low values of TKE and TDR occur together perhaps because the core flow flip-flops between quiescent and turbulent states as show in Kwon *et al.* (2014). However, the zero average time lag of plane-average dynamics is seemingly inconsistent with the time lag discovered in volume-average dynamics in §3.1. It is therefore natural to question if plane-average TKE at some distance from the wall correlates with plane-average TDR at another distance from the wall, with or without time lag.

### 3.3. *2-time 2-plane correlations: TKE and TDR*

To unveil the time lag observed in figure 1 and to illuminate the dynamic relation between TKE and TDR (as well as TPR and TDR) in space and time, we now investigate 2-time 2-plane correlations. The correlations between TKE at a reference $x$-$z$ plane and TDR at another plane in the channel are defined as follows:

$$\rho_{[\varepsilon,E^{\mathrm{ref}}]}(\tau, y; y^{\mathrm{ref}}) = \frac{\overline{\varepsilon'(t+\tau, y)E'(t, y^{\mathrm{ref}})}}{\sqrt{\overline{\varepsilon'^2(t, y)}}\,\sqrt{\overline{E'^2(t, y^{\mathrm{ref}})}}}. \tag{3.5}$$

A similar 2-time 2-plane correlation can be defined by replacing TKE with TPR, i.e. $E^{\mathrm{ref}}$ with $P^{\mathrm{ref}}$ and $E'$ with $P'$. From the 2-time 1-plane correlations between TKE and TDR in figure 3($a, c, e, g, i$), we observe a region of low positive correlations between $y/H = 0.2$ and $y/H = 0.4$, the outer part of the near-equilibrium ($\overline{P} \approx \overline{\varepsilon}$) region. We therefore start by plotting the correlation contours for reference plane $y^{\mathrm{ref}}/H = 0.3$ which is where the minimal 2-time 1-plane correlation at zero time lag is found (figure 3). Taking a different reference plane within this low correlation region $y/H = 0.2$ to $y/H = 0.4$ changes little the observations that follow throughout the paper.

The correlation contours in $(\tau, y)$ space, with TKE at reference plane $y^{\mathrm{ref}}/H = 0.3$, are plotted in figure 4 for the five Reynolds numbers considered. It can be clearly observed that the TKE in the near-equilibrium region correlates with TDR in both the core region and the near-wall region, with a positive time lag and also a wall-distance lag. This observed

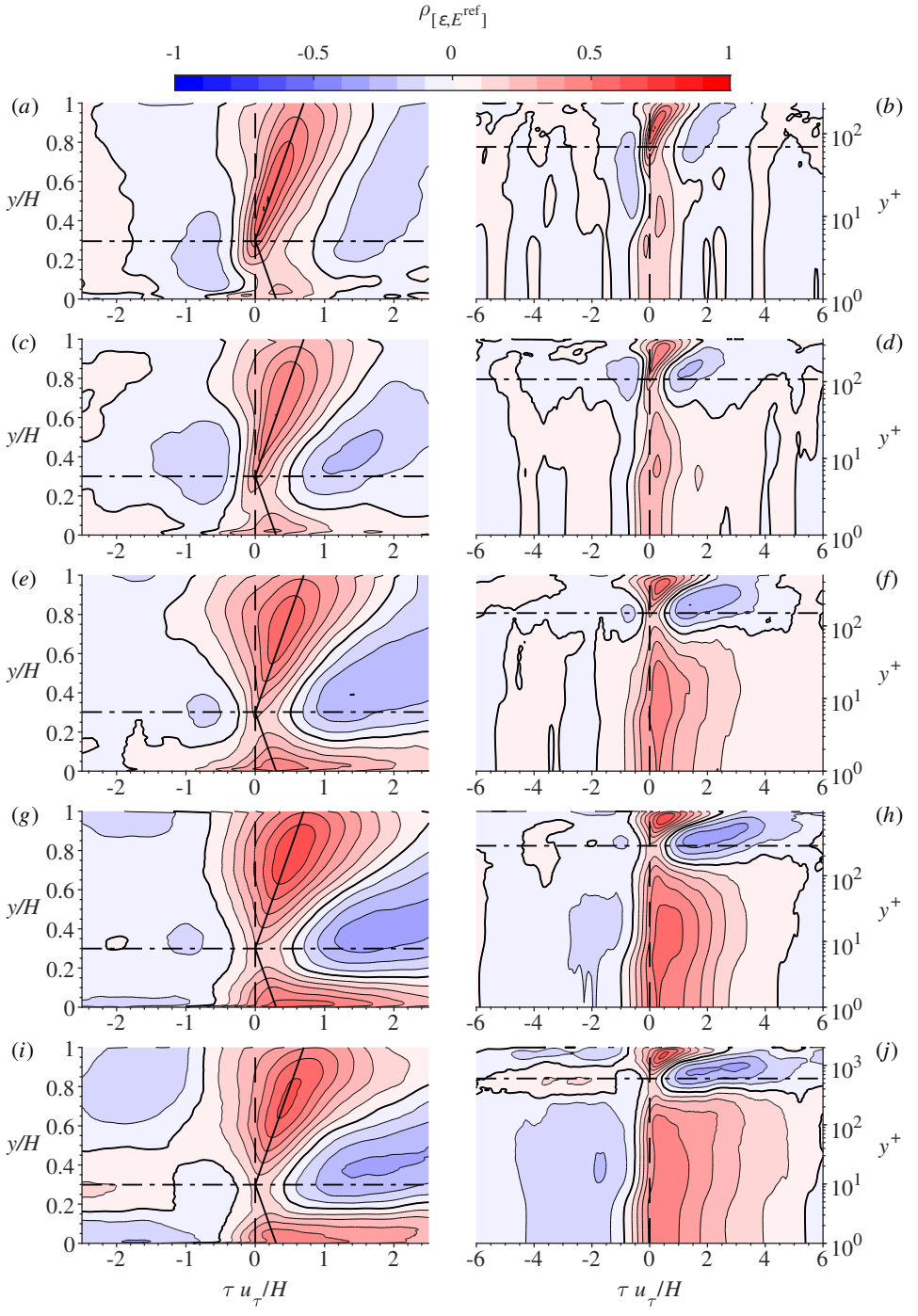



Figure 4: 2-time 2-plane correlation function contours $\rho_{[\varepsilon,E^{\mathrm{ref}}]}$ versus distance from the wall $y^+$ or $y/H$ and time lag $\tau u_\tau/H$ with respect to TKE at the reference plane $y^{\mathrm{ref}}/H = 0.3$ (horizontal dash-dotted lines). The slopes of the solid black lines are $\pm u_\tau$ respectively. $(a, b)$ R230, $(c, d)$ R360, $(e, f)$ R500, $(g, h)$ R950, $(i, j)$ R2000. Vertical dashed lines, $\tau = 0$.

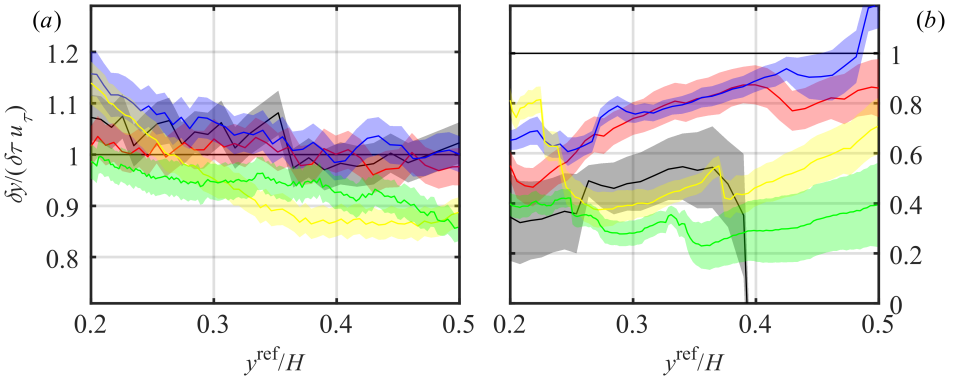



Figure 5: For given $y^{\mathrm{ref}}$, one defines $\delta y(y, y^{\mathrm{ref}}) \equiv |y - y^{\mathrm{ref}}|$, and then extracts $\delta\tau$ from the maximum correlation at local $y$ and $y^{\mathrm{ref}}$, i.e.: $\rho(\delta\tau, y; y^{\mathrm{ref}}) = \sup_\tau\{\rho(\tau, y; y^{\mathrm{ref}})\}$, where $\rho$ is defined in equation (3.5). A best linear fit of $\delta y$ versus $\delta\tau$ gives an average slope $\delta y/\delta\tau$ with its 95% confidence interval for each $y^{\mathrm{ref}}$. We plot the fitted slopes $\delta y/(\delta\tau u_\tau)$ as a function of $y^{\mathrm{ref}}$ $(a)$ for the 2-time 2-plane correlations above the reference plane and $(b)$ for the 2-time 2-plane correlations below the reference plane. In both $(a)$ and $(b)$ the shading around the different-coloured lines are 95% confidence intervals for R230 (black line), R360 (red line), R500 (blue line), R950 (yellow line) and R2000 (green line).

time lag resolves the discrepancy between volume-average correlations and 2-time 1-plane correlations. Along the path of positive correlation from the reference plane towards the channel centre, the peaks of correlations in $(\tau, y)$ space lie very close to a line of slope $\delta y/\delta\tau = (1 \pm 0.2)u_\tau$ (see figure 4 and 5$a$). This is a time lag combined with a wall-distance lag and the ratio of the latter to the former is $\sim u_\tau$. Note that any turbulence transport in the wall-normal direction should be through the wall-normal velocity in the turbulent transport term (see $T_t(y, t)$). The mean wall-normal velocity is zero but the standard deviation of the wall-normal velocity fluctuations $v_{\mathrm{rms}}$ is of order $u_\tau$ and varies slowly with $y$. The correlations with time lag in figure 4 cannot be caused by the passage of inclined structures previously observed in turbulent boundary layers (e.g. in Marusic & Heuer 2007) and FD TCF (e.g. in Cheng *et al.* 2022). If they were, TDR in the core region would precede TKE in the near-equilibrium region due to the earlier passage of structures further away from the wall than closer to the wall.

TKE can be transported both upwards and downwards from the reference plane. During wall-normal turbulence transport, high TKE fluctuations are also transferred towards smaller scales which leads to high TDR fluctuations. This transport through scales is illustrated by the increasing correlation between TKE and TDR further away from the reference plane (figure 4) as well as by the path of the slowest decorrelation of TKE with itself which is also along the line of slope $\delta y/\delta\tau \approx u_\tau$ (not shown here). This interpretation is supported by figure 6 which shows that the 2-time 2-plane correlation between TPR and TDR behaves differently even though the volume-average TPR has similar time lag with volume-average TDR as volume-average TKE. The difference between figures 4 and 6 can be understood with the fact that TPR is not transported through space and scales whereas TKE is. Figure 6 shows that TPR and TDR are maximally correlated locally rather than non-locally along a $\delta y/\delta\tau$ line as in the case of TKE and TDR in figure 4.

Regarding the path of high correlations towards the core region, the velocity $\delta y/\delta\tau$ is close to that of the plane-average ejections found by Flores & Jiménez (2010). In the core region, the mean shear is very weak and the eddies are mainly composed of dissipative ones (see §3.2). It is, therefore, conceivable that this path is associated with the energy cascade initiated from the large-scale structure mainly around $y^{\mathrm{ref}}/H = 0.3$. This would also

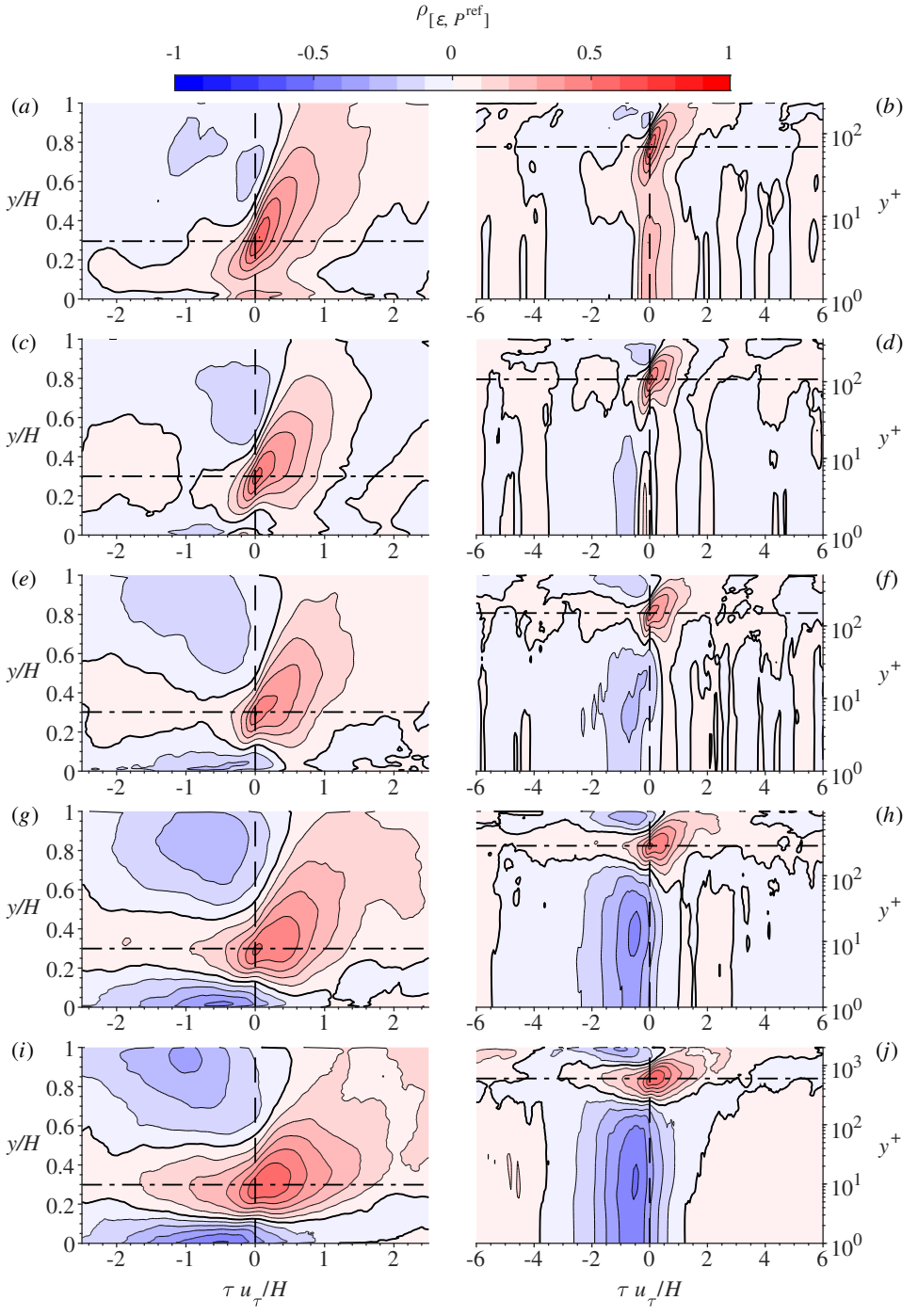



Figure 6: 2-time 2-plane correlation function contours $\rho_{[\varepsilon,P^{\mathrm{ref}}]}$ versus distance from the wall $y^+$ or $y/H$ and time lag $\tau u_\tau/H$ with respect to TPR at the reference plane $y^{\mathrm{ref}}/H = 0.3$ (horizontal dash-dotted lines). $(a, b)$ R230, $(c, d)$ R360, $(e, f)$ R500, $(g, h)$ R950, $(i, j)$ R2000. Vertical dashed lines, $\tau = 0$.

imply that the ejections towards the outer region (Flores & Jiménez 2010) involve not only momentum transport but also energy transport in space and in scales, which leads to TDR fluctuations through a cascade process. In the path towards the wall, the correlation velocity $\delta y/\delta\tau$ appears to be smaller than $(1 \pm 0.2)u_\tau$ and less well-defined (see figure 5*b*). The contours in figure 4 show that as $Re_\tau$ increases, the TKE in the near-equilibrium region and the TDR in the near-wall region correlate with a wider and more skewed spread of time lags in $H/u_\tau$ units. It is worth emphasising that this TKE to TDR spatio-temporal path towards the wall is fundamentally different from the superposition and modulation effects described in Hutchins & Marusic (2007*b*).

As in §3.2, we observe from the 2-time 2-plane correlation in figure 4 a region of anti-correlation between turbulence dissipation rate and TKE around the reference plane at $y^{\mathrm{ref}} = 0.3H$. The extent of this anti-correlation shows a spread of time lags beyond $\tau u_\tau/H \simeq 0.5$ and little wall-distance lag, consistent with the anti-correlation in 2-time 1-plane correlation in figure 3. This anti-correlation signifies a high/low TKE event followed in time by low/high dissipation around a reference plane taken at the outer edge of the near-equilibrium region. A plausible explanation of the local anti-corelation between TKE and TDR with time lag could be that TKE is transported away from the upper near-equilibrium region and therefore does not remain there to cascade and dissipate. A high instance of TKE at the upper near-equilibrium region is therefore followed by no increase in dissipation, in fact even a decrease in dissipation given that there is no local cascade at $y \approx y^{\mathrm{ref}}$ between $y/H = 0.2$ and $y/H = 0.4$ to feed it.

As a side note, unlike the peak of 2-time 1-plane correlation located at the channel centre in figure 3, the maximum 2-time 2-plane correlation only reaches a distance from the wall around $y \sim 0.75H$, above which TKE at the reference plane decorrelates with TDR in the core region. This observed decorrelation is likely due to the fact that the single core region in FD TCF contains information such as signals of TKE ejected from both the upper channel and the lower channel. It would be interesting to investigate in the future temporal correlations between TKE in the near-equilibrium layer and TDR in the outer layer of wall-bounded turbulence with only one wall, such as that of open channel flow (Yao *et al.* 2022; Pirozzoli 2023) or turbulent boundary layers.

### 3.4. *2-time 2-plane correlations: near-wall region and Reynolds number dependence*

The observations made in §3.3 indicate a correlation velocity closely related to the turbulent transport velocities from the near-equilibrium region both towards and away from the wall. The path of correlation away from the wall shows little dependence on the Reynolds number and is always very close to the friction velocity. However, the correlation between the TKE in the near-equilibrium region and the TDR in the near-wall region is heavily dependent on Reynolds number. We therefore turn our focus on the 2-time 2-plane correlations between TKE at a reference plane taken in the near-wall region and TDR fluctuations elsewhere. The correlation contours with reference plane taken at $y^{\mathrm{ref}} = 10\delta_\nu$ are presented in figure 7. This figure does not change sinificantly if we take a different reference plane in the range $y^{\mathrm{ref}} \in [10, 50]\delta_\nu$.

The first point made by figure 7 is that TKE and TDR fluctuations are strongly correlated in the near-wall region below $y^+ \approx 100$, without time lag on average but also, quite symmetrically, with equally positive and negative time lags in the range $-2 \leqslant \tau u_\tau/H \leqslant 2$. This strong correlation makes sense given that the length and velocity scales associated with TKE and TDR are not well separated in the near-wall region. The second observation coming out of figure 7 is that, unlike figure 4, no continuous path of positive correlation exists from the near wall to the near-equilibrium region and ultimately to the core region. And the third

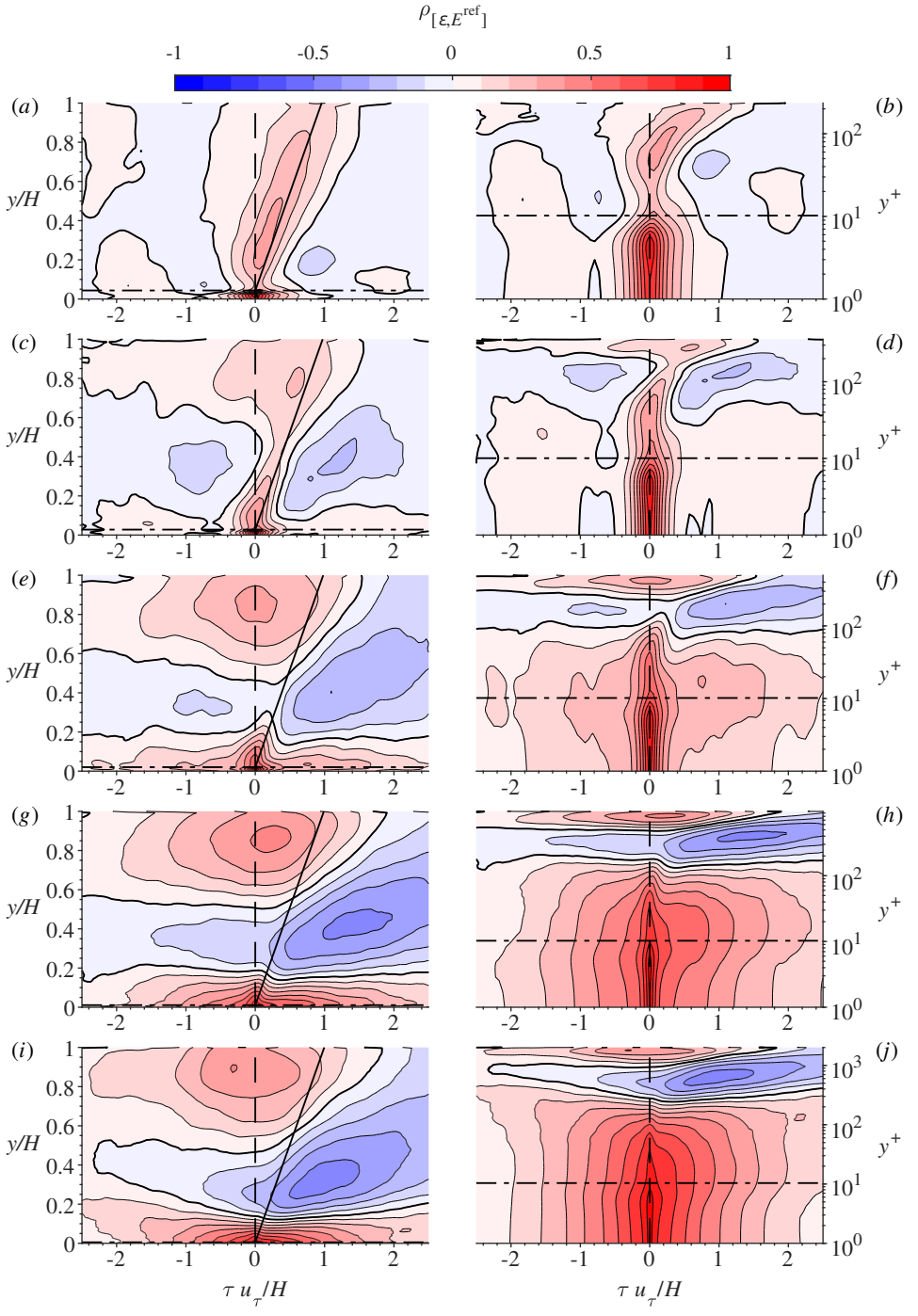



Figure 7: 2-time 2-plane correlation function contours $\rho_{[\varepsilon,E^{\mathrm{ref}}]}$ versus distance from the wall $y^+$ or $y/H$ and time lag $\tau u_\tau/H$ with respect to TKE at the reference plane $y^{\mathrm{ref}} = 10\delta_\nu$ (horizontal dash-dotted lines). The slopes of the solid black lines are $\pm u_\tau$ respectively. $(a, b)$ R230, $(c, d)$ R360, $(e, f)$ R500, $(g, h)$ R950, $(i, j)$ R2000. Vertical dashed lines, $\tau = 0$.

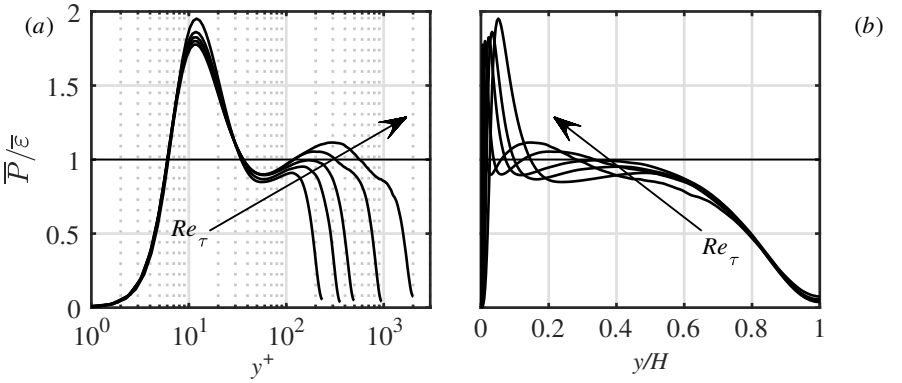



Figure 8: Time-average mean profile of TPR over TDR in ($a$) inner unit and ($b$) outer unit for five Reynolds numbers. Horizontal solid line indicates $\overline{P}/\overline{\varepsilon} = 1$.

observation is the significant positive correlation without significant time lag between TKE in the near-wall region and TDR in the core region.

For a start towards an interpretation of this third observation, we plot in figure 8 the ratio between the time-average TPR over the time-average TDR in inner and outer units obtained from our data. The notion of "equilibrium" is merely an approximation of the actual TKE budget in the overlap region. The outer peak of the production to dissipation ratio increases with Reynolds number, and moves away from the wall in inner units. This is a signature of the very-large-scale motions at moderately high Reynolds number (Kim & Adrian 1999). As these outer structures become stronger with increasing Reynolds number, their contributions to the fluctuations in the TKE budget may also become more pronounced. These strong outer structures in the near-equilibrium region become increasingly dominant in both outer and near-wall TDR fluctuations. In the near-wall region, TKE and TDR fluctuate almost in the same manner (as seen from the high correlation with no time lag on average in the near-wall region in figure 7). Strong correlations between TKE near the wall and TDR in the core region therefore also indicate strong correlations between TDR near the wall and TDR in the core region with zero or little time lag at high Reynolds number, both presumably controlled by strong energy-containing structures of sizes comparable to the channel half height. Indeed, the 2-time 2-plane correlations of TDR at $y^+ = 10$ and TDR at other wall-distances $y$ (not shown here for economy of space) are nearly identical to figure 7 except perhaps at the lowest $Re_\tau = 230$ for which they are just very similar. A correlation where the reference TKE is taken in the core region was also computed (not shown here for economy of space) and similar instantaneous correlation values with the near-wall TDR were found, suggesting that the near-wall TDR and the core TDR are both controlled by structures of sizes comparable to the channel half height.

### 3.5. *2-time 2-plane correlations: ejections and sweeps*

As already mentioned in subsection 3.3, the spatio-temporal path of TKE to TDR from the near-equilibrium region to the outer region observed in that subsection is reminiscent of the spatio-temporal path of ejections/sweeps oberved by (Flores & Jiménez 2010). Hence, we now focus on the regions in the $x$-$z$ plane where ejections and sweeps happen. For any quantity $Z(x, y, z, t)$ in FD TCF, we define a conditional plane-average as

$$Z_{\mathrm{Qs}}(y,t) = \frac{1}{A_{\mathrm{Qs}}(y,t)} \iint_{\mathrm{Qs}} Z(x,y,z,t)\, \mathrm{d}x\, \mathrm{d}z, \tag{3.6}$$

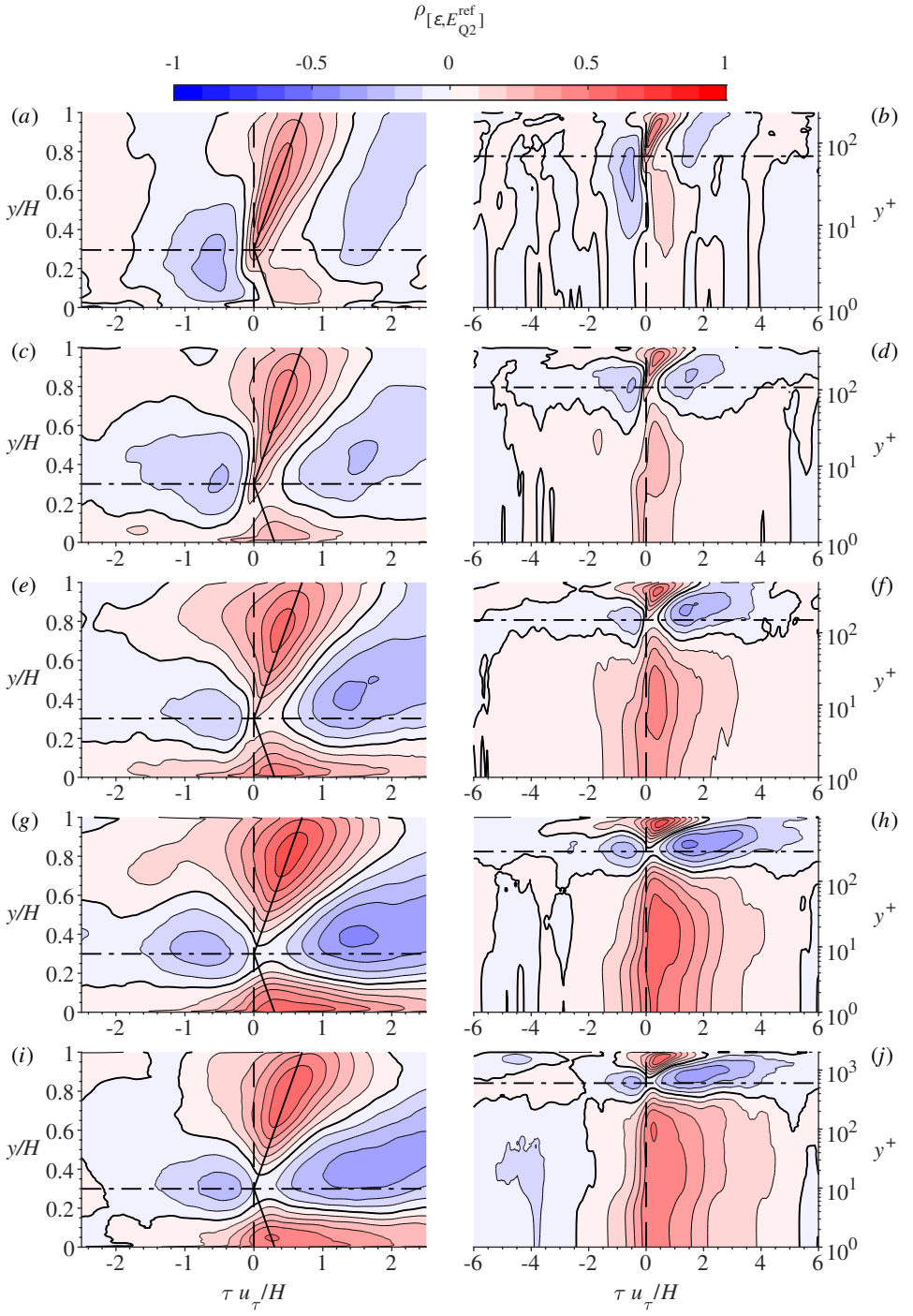



Figure 9: 2-time 2-plane correlation function contours $\rho_{[\varepsilon,E_{Q2}^{ref}]}$ versus distance from the wall $y^+$ or $y/H$ and time lag $\tau u_\tau/H$ with respect to TKE conditioned on ejection event at the reference plane $y^{ref}/H = 0.3$ (horizontal dash-dotted lines). The slopes of the solid black lines are $\pm u_\tau$ respectively. $(a, b)$ R230, $(c, d)$ R360, $(e, f)$ R500, $(g, h)$ R950, $(i, j)$ R2000. Vertical dashed lines, $\tau = 0$.

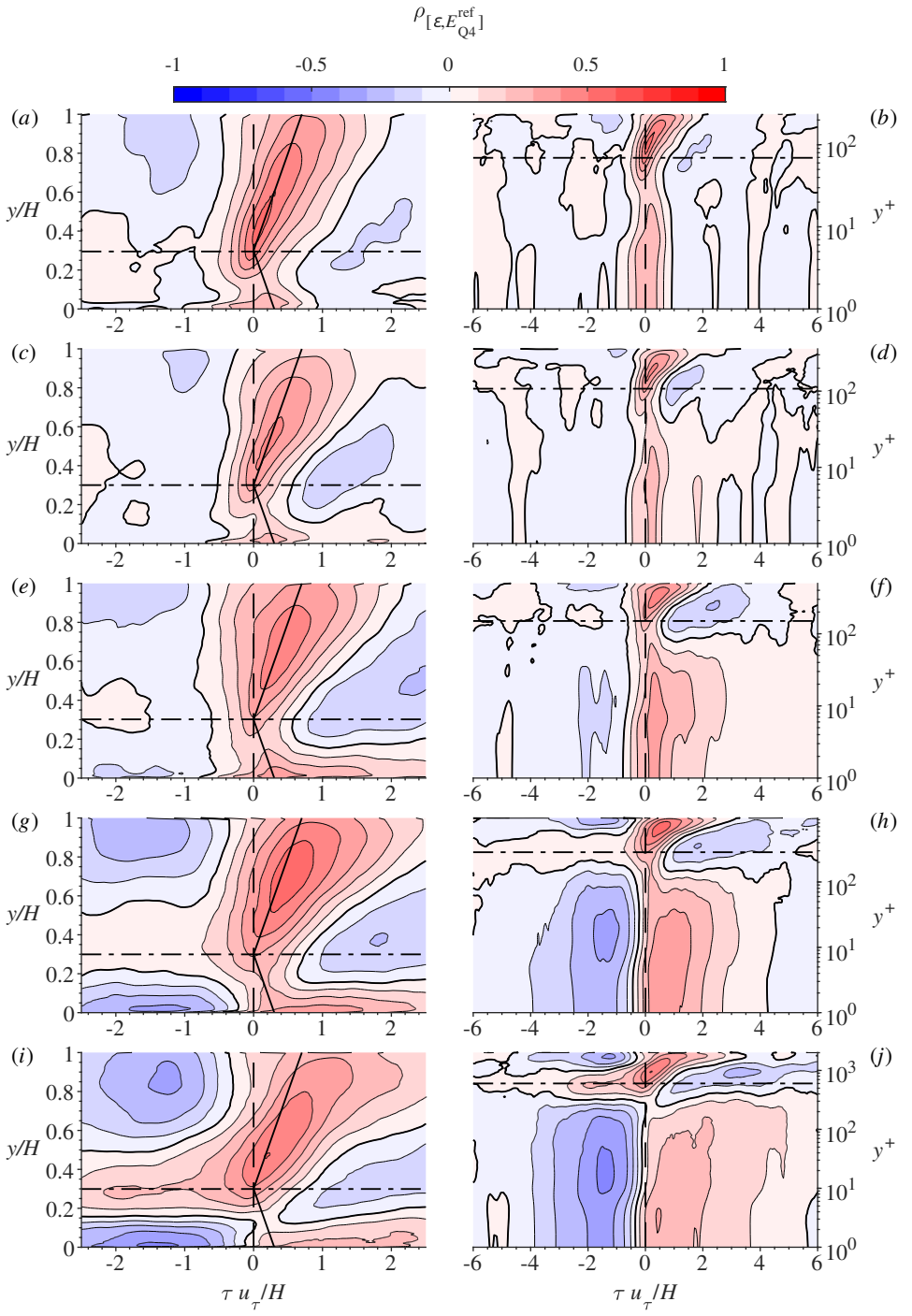



Figure 10: 2-time 2-plane correlation function contours $\rho_{[\varepsilon,E_{Q4}^{ref}]}$ versus distance from the wall $y^+$ or $y/H$ and time lag $\tau u_\tau/H$ with respect to TKE conditioned on sweep event at the reference plane $y^{ref}/H = 0.3$ (horizontal dash-dotted lines). The slopes of the solid black lines are $\pm u_\tau$ respectively. $(a, b)$ R230, $(c, d)$ R360, $(e, f)$ R500, $(g, h)$ R950, $(i, j)$ R2000. Vertical dashed lines, $\tau = 0$.

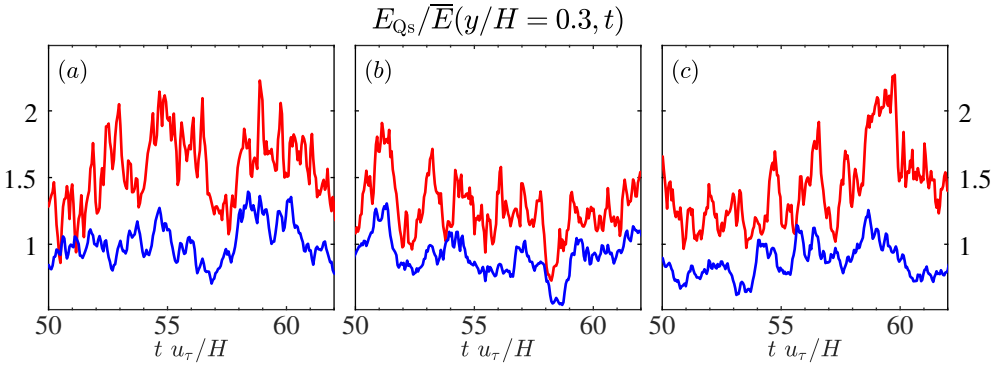



Figure 11: Time evolution of conditionally averaged TKE $E_{\mathrm{Qs}}/\overline{E}$ at $y/H = 0.3$, normalised by plane- and time-averaged TKE, in the lower half channel. Red signals indicate TKE conditionally averaged over ejections (s=2) and blue over sweeps (s=4). (*a*) R500, (*b*) R950, and (*c*) R2000.

where Qs, for s = 1, 2, 3, 4, indicates the four quadrants in the $u$-$v$ plane and $A_{\mathrm{Qs}} = A_{\mathrm{Qs}}(y, t)$ is the sum of the areas in the $x$-$z$ plane where Qs events take place (Wallace *et al.* 1972; Willmarth & Lu 1972). In particular, we investigate 2-time 2-plane correlations of unconditioned TDR with TKE conditionally averaged either over ejections (Q2) or over sweeps (Q4) in each plane. It is well-known that ejections and sweeps are the principal contributors to the Reynolds stress $-\langle u'v'\rangle$ in the near-equilibrium region (Willmarth & Lu 1972).

Figure 9 presents the same correlation function as in (3.5) but using unconditioned TDR and TKE conditionally averaged (as in equation 3.6) over Q2 ejection events, i.e. locations in the plane where $u' < 0$ and $v' > 0$. The resulting correlation contours show a trend consistent with the unconditional TKE and TDR in figure 4 (in particular, very similar correlation velocities $\delta y/\delta\tau$ to within 10% and correlation levels comparable to the unconditional correlations to within 7%).

When the correlation function is computed using TKE conditionally averaged over Q4 sweep events ($u' > 0$ and $v' < 0$) as shown in figure 10, noticeable changes in the correlation velocity and in the value of correlation coefficients appear. The spatio-temporal path towards the core region shows a significantly reduced correlation velocity (by up to 33% reduced) and significantly reduced levels of correlation (by up to 20% reduced). The, perhaps counter-intuitive, observation, however, is the difference of the correlation coefficients between the ejection-conditioned and sweep-conditioned correlations in the near-wall region. Sweep events are $v' < 0$ events, which in effect transport high streamwise momentum ($u' > 0$) towards the wall. They may, therefore, be expected to be mainly responsible for the dissipation of the near-wall region, hence the TKE and TDR conditionally averaged over sweep events may be expected to be more strongly correlated with higher correlation coefficient near the wall. The present correlation contours are contrary to this expectation. Even though ejection events correspond to $v' > 0$ structures which would mainly transport slow ($u' < 0$) streamwise momentum away from the wall, they appear to be better correlated with the near-wall dissipation than sweep events. For the higher three Reynolds numbers, the correlation levels between reference ejection-conditioned TKE and near-wall TDR (figure 9$f, h, j$) varies within 10% from the unconditional correlation (figure 4$f, h, j$), whereas the sweep-conditioned correlation levels (figure 10$f, h, j$) are reduced by 20% to 36%.

In FD TCF, the plane-average wall-normal velocity must satisfy $\langle v\rangle\,(y, t) = 0$, an exact result imposed by the no-penetration boundary condition, homogeneity in the wall-parallel directions and incompressibility. This suggests that locally positive $v' > 0$ and negative

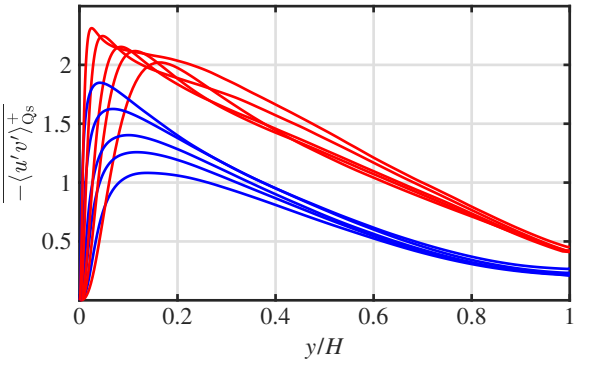



Figure 12: Time-average mean profile of conditionally averaged Reynolds shear stress over ejections (red lines) and sweeps (blue lines) for five Reynolds numbers.

$v' < 0$ must occur in pairs at any wall-parallel plane in the channel. As a result, ejections and sweeps should also happen simultaneously at any plane, and the TKE conditionally averaged over ejections and sweeps should fluctuate more or less concurrently as appears to be approximately the case (see figure 11). On the other hand, it is worth pointing out that ejections have previously been shown to provide the largest contribution to the overall Reynolds shear stress and TKE (Willmarth & Lu 1972). From figure 11, in the near-equilibrium region, the TKE conditionally averaged over ejections is indeed higher than conditionally averaged over sweeps, indicating that local turbulent motions associated with ejections are more energetic than sweeps (Farano *et al.* 2017), which might be responsible for the faster correlation velocity than that of sweeps towards the core region.

In the near-wall region, there is little separation between energy containing length scales and dissipative length scales. Turbulence energetics, whether it being the TKE or dissipation, plane-average or conditionally averaged over ejections/sweeps, are expected to fluctuate concurrently near the wall. While we expect the sweeps to be responsible for the near-wall fluctuations, it is actually the ejections in the near-equilibrium regions that correlate with the near-wall dissipation better, contrary to our expectation. We present here an hypothesis to account for this observation. Ejections and sweeps operating in tandem, anything relating to one should also somehow relate to the other. Presumably, sweeps are responsible for the connection and travel to the wall and ejections for the connection and travel to the core, but correlations conditioned on ejections are stronger than correlations conditioned on sweeps because ejections are more organised/structured than sweeps. In support of this suggestion, we plot in figure 12 the time-average mean profile of conditionally plane-average Reynolds shear stress over ejections and over sweeps respectively. One may consider the Reynolds shear stress as an indication of organisation/coherence given that $-\langle u'v'\rangle = 0$ if $u'$ and $v'$ are uncorrelated as expected in the absence of organised coherent flow structure, and therefore higher absolute values of $-\langle u'v'\rangle$ indicate higher order/coherence. In the case of FD TCF, the magnitude of $\overline{-\langle u'v'\rangle_{Q2}}$ (time-average $-\langle u'v'\rangle$ conditioned on Q2 i.e. plane-averaged over Q2 regions only) is significantly larger than $\overline{-\langle u'v'\rangle_{Q4}}$ for $y > 0.2H$, thereby suggesting that ejections are more organised than sweeps. As a result the correlations conditioned on ejections in figure 9 are stronger than the correlations conditioned on sweeps in figure 10 both towards the wall and towards the core. Note that significant correlations conditioned on sweeps also appear towards the core region in figure 10 which is as counter-intuitive as the significant correlations conditioned on ejections towards the wall in figure 9.

## 4. Dynamics of TPR

Having examined the links between TKE and TDR fluctuations we now turn to the production of TKE which, anyway, occurs before its dissipation. One, of course, expects the volume-average TPR to lead the volume-averaged TKE simply because TKE builds up as an integration in time of TPR (see (3.2). This is confirmed by the cross-correlation function $\rho_{[P_V,E_V]}$ (red line in figure 1$c, f, i, l, o$): the peaks of the correlations are around $\tau u_\tau/H \sim -0.1$ (time lead) with values of $\rho_{[P_V,E_V]}$ between 0.5 and 0.8 (increasing with $Re_\tau$). The 2-time 1-plane correlation $\rho_{[P,E]}$ (not shown here for brevity) calculated as in equation (3.4) by replacing TDR $\varepsilon$ with TPR $P$, shows little/no average time lag between the plane-average TPR and the plane-average TKE, suggesting that the dynamic relation between TPR and TKE is more complex than expected.

In §4.1, we therefore investigate the 2-time 2-plane correlation $\rho_{[P,E^{\mathrm{ref}}]}$ between TKE at reference plane $y^{\mathrm{ref}}/H = 0.3$ (chosen indicatively as results are very similar for any $y^{\mathrm{ref}}/H$ between 0.2 and 0.4) and TPR elsewhere. TPR fluctuations result from fluctuations of mean shear and Reynolds shear stress and we therefore concentrate on both in §4.2 and §4.3. A mechanistic model is proposed in §4.3 to explain the dynamics relating TPR and TKE.

### 4.1. *2-time 2-plane correlation: TPR and TKE*

We plot in figure 13 the 2-time 2-plane correlation between TKE at reference plane $y^{\mathrm{ref}} = 0.3H$ and TPR elsewhere. Positive correlations exist between TKE at the reference plane and TPR in the near-wall and TPR in the core region. The correlations in the core region share similar peak locations as those between TKE and TDR (figure 4), but the levels of correlation between TKE and TPR are significantly lower and the correlation peaks do not follow the $\delta y/\delta\tau \approx u_\tau$ line which characterises the path from TKE to TDR. The core correlation between TKE and TPR must be rooted in the correlation between TKE and Reynolds shear stress (see §4.2).

The positive correlations between TKE at the reference plane and TPR in the near-wall region appear similar to the correlations between TKE at the same reference plane and TDR in the near-wall region (see figure 4) in terms of both the levels of correlations and the peak locations of the correlations, i.e. the average time lags. As discussed in §3.2, §3.4 and §3.5, the near-wall dynamics are limited by a small range of scales and TKE, TDR and TPR fluctuate almost concurrently near the wall. The similarity between correlations $\rho_{[P,E^{\mathrm{ref}}]}$ and $\rho_{[\varepsilon,E^{\mathrm{ref}}]}$ near the wall is therefore expected. One observation is that the near-wall production depends on the turbulent energy further away from the wall, which becomes more evident at higher Reynolds numbers (increasing levels of correlation in the near-wall region). The peaks of the correlation with time lag instead of time lead indicate that the near-wall TPR lags the reference TKE. Such an observation may be unexpected, since one often views the turbulence production as a source of turbulent energy and TPR should lead TKE in time, as shown in a volume-average sense in §3.1.

It is worth pointing out that the 2-time 2-plane correlations with time lags in figure 13 are not inconsistent with the time lead of peak $\rho_{[P_V,E_V]}$ observed in the volume-average correlation. The observed positive values in figure 13 of 2-time 2-plane correlations with time lag in the near-wall and core regions largely cancel the negative values of 2-time 2-plane correlations with time lag in the near-equilibrium region when integrated in the wall-normal direction, and the overall time-lagged peaks of correlations are attenuated.

### 4.2. *2-time 2-plane correlation: Reynolds shear stress and TKE*

The time-fluctuating TPR is the product of the time-fluctuating plane-average mean streamwise shear and the time-fluctuating plane-average Reynolds shear stress $-\langle u'v'\rangle$. (The

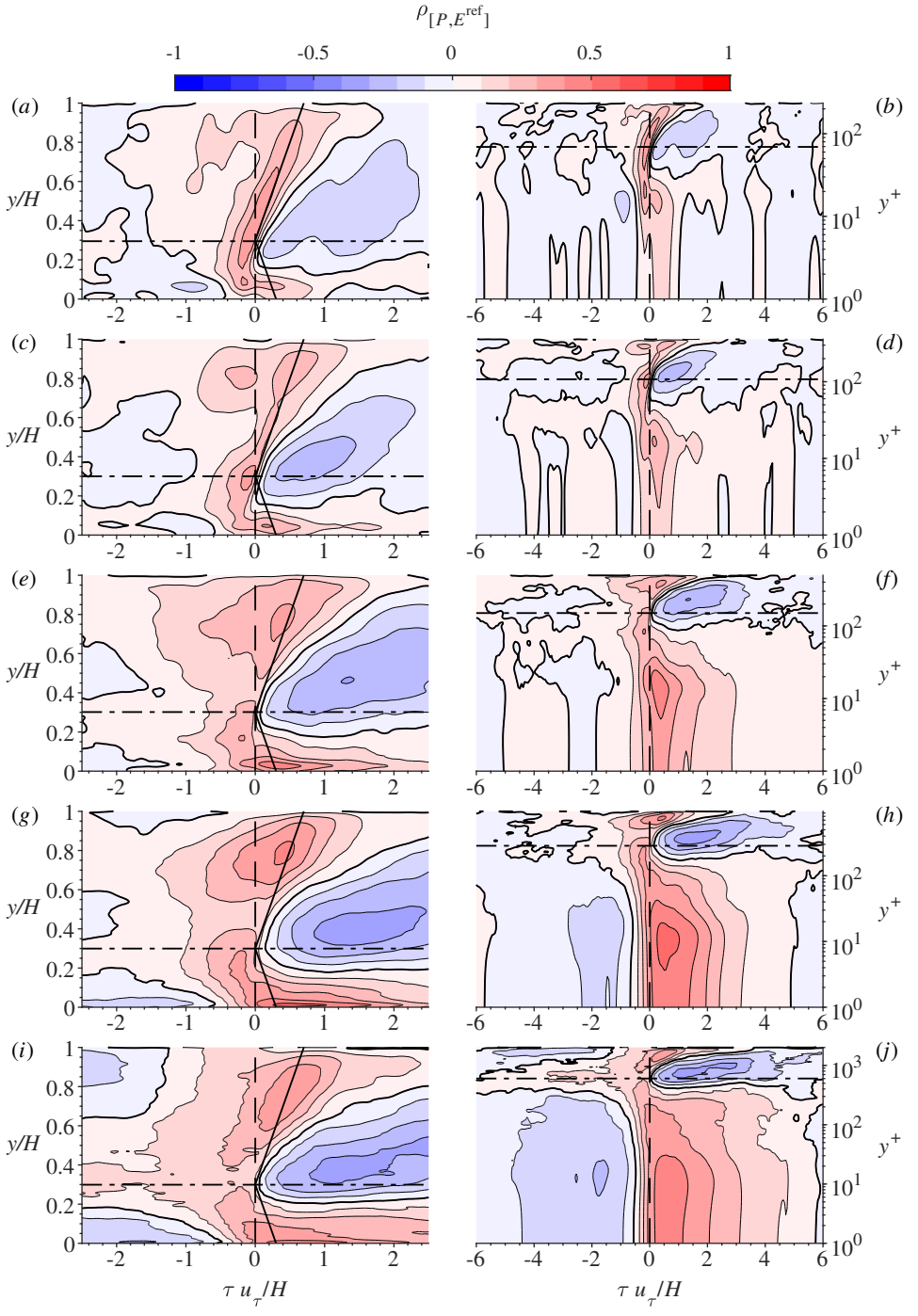



Figure 13: 2-time 2-plane correlation function contours $\rho_{[P,E^{\mathrm{ref}}]}$ versus distance from the wall $y^+$ or $y/H$ and time lag $\tau u_\tau/H$ with respect to TKE at the reference plane $y^{\mathrm{ref}}/H = 0.3$ (horizontal dash-dotted lines). The slopes of the solid black lines are $\pm u_\tau$ respectively. $(a, b)$ R230, $(c, d)$ R360, $(e, f)$ R500, $(g, h)$ R950, $(i, j)$ R2000. Vertical dashed lines, $\tau = 0$.

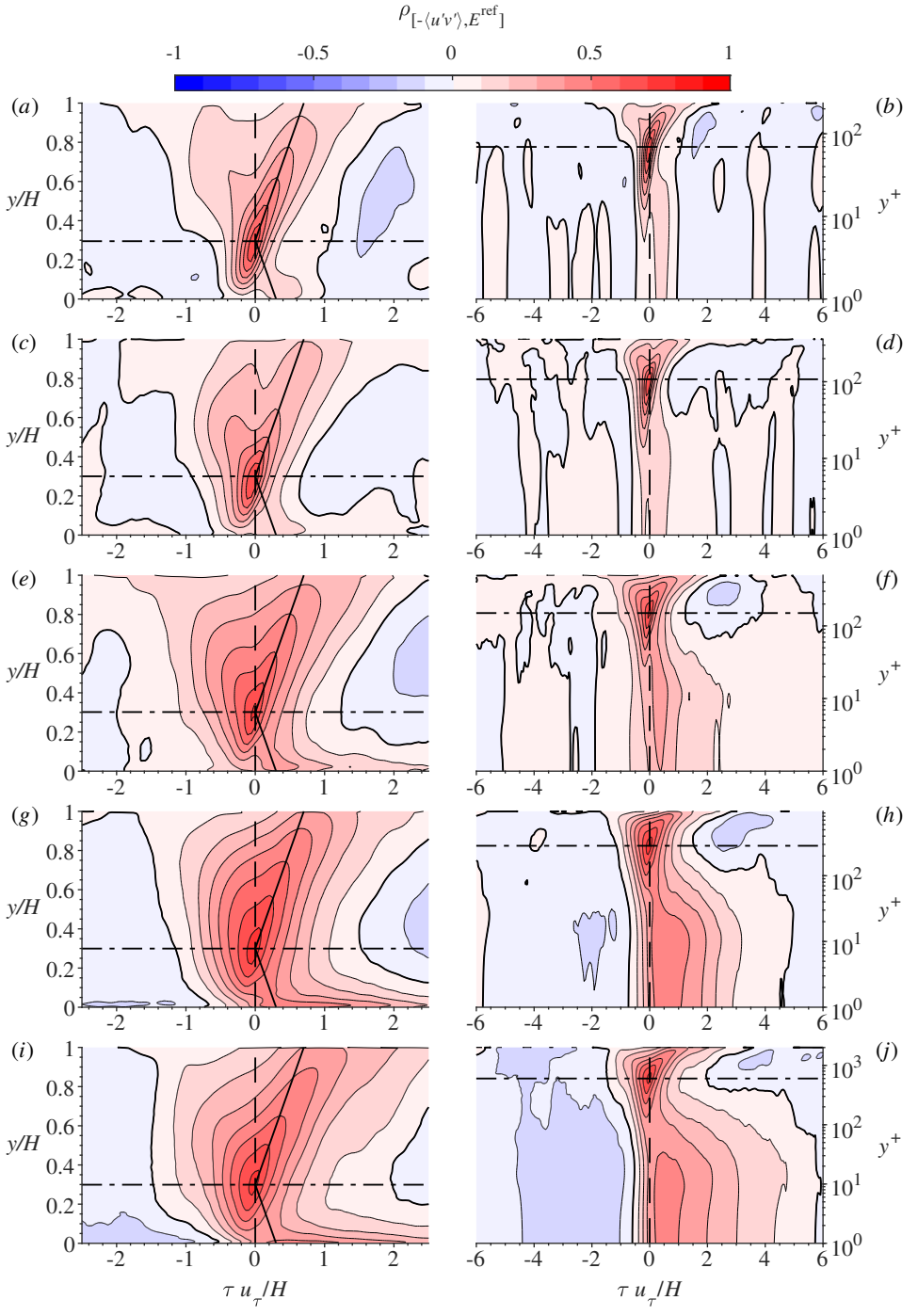



Figure 14: 2-time 2-plane correlation function contours $\rho_{[-\langle u'v'\rangle, E^{\mathrm{ref}}]}$ versus distance from the wall $y^+$ or $y/H$ and time lag $\tau u_\tau/H$ with respect to TKE at the reference plane $y^{\mathrm{ref}}/H = 0.3$ (horizontal dash-dotted lines). The slopes of the solid black lines are $\pm u_\tau$. $(a, b)$ R230, $(c, d)$ R360, $(e, f)$ R500, $(g, h)$ R950, $(i, j)$ R2000. Vertical dashed lines, $\tau = 0$.

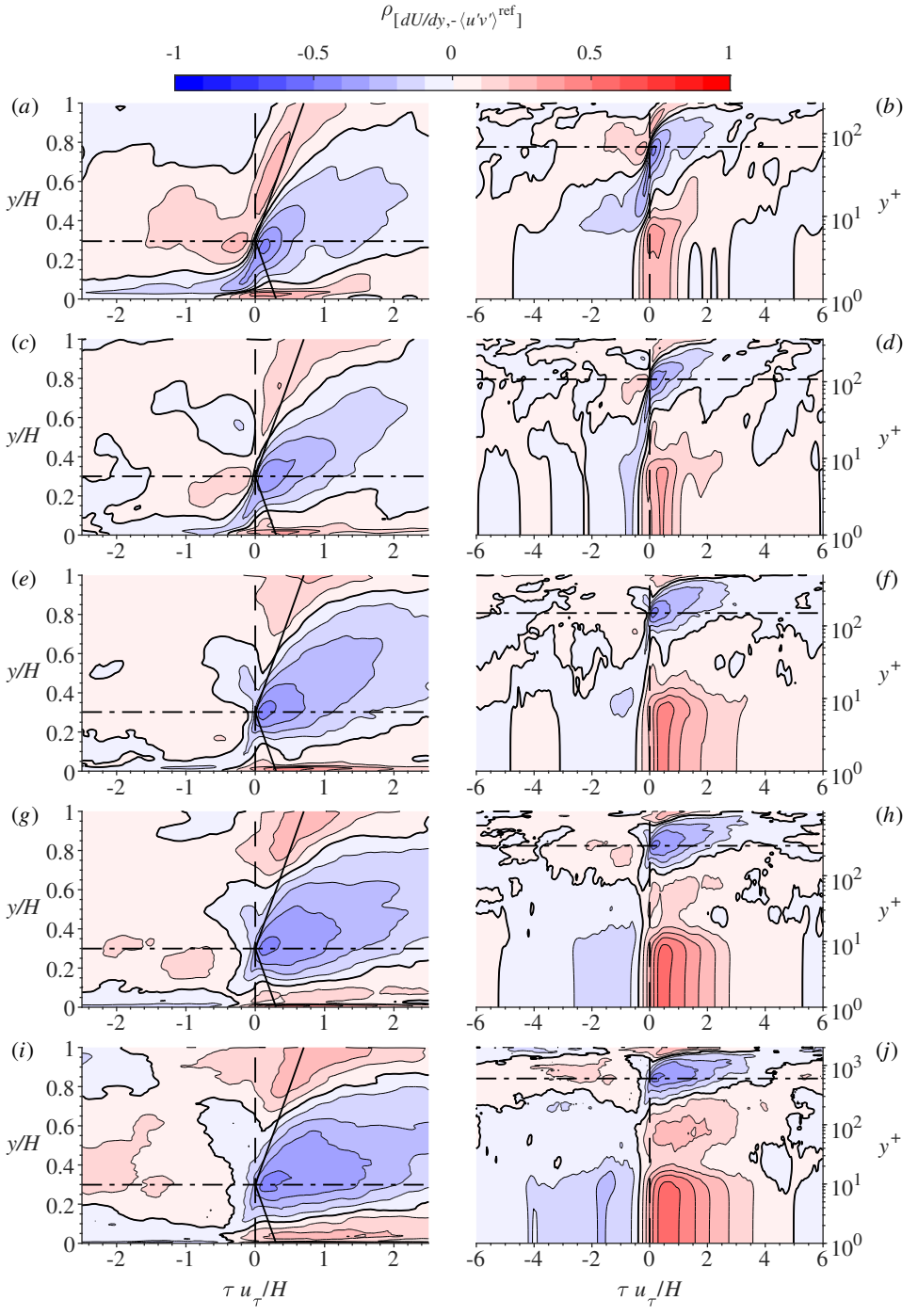



Figure 15: 2-time 2-plane correlation function contours $\rho_{[dU/dy,-\langle u'v'\rangle^{\mathrm{ref}}]}$ versus distance from the wall $y^+$ or $y/H$ and time lag $\tau u_\tau/H$ with respect to plane averaged Reynolds shear stress at the reference plane $y^{\mathrm{ref}}/H = 0.3$ (horizontal dash-dotted lines). The slopes of the solid black lines are $\pm u_\tau$ respectively. $(a, b)$ R230, $(c, d)$ R360, $(e, f)$ R500, $(g, h)$ R950, $(i, j)$ R2000. Vertical dashed lines, $\tau = 0$.

contribution from the plane-average spanwise mean shear and the corresponding Reynolds shear stress component $-\langle u'w'\rangle$ is minimal compared to the streamwise component, less than 1% of the overall production). We therefore analyse the dynamics of the turbulence production in terms of 2-time 2-plane correlations between the TKE at the reference plane and these two factors.

The TKE and the Reynolds shear stress are closely related to each other in terms of their time fluctuations. As shown by the correlation plot $\rho_{[-\langle u'v'\rangle, E^{\mathrm{ref}}]}$ in figure 14, the TKE and the Reynold shear stress are maximally correlated around the reference plane with no average time lag. The correlation contours above the reference plane show both wall-distance lag and time lag along a line of slowest decorrelation that is very close to the friction velocity up to around $y = 0.8H$. In the near-wall region around the viscous sublayer, as Reynolds number increases, positive correlations develop with time lag, the spread of which widens in outer time unit $H/u_\tau$, and the levels of correlations increases.

Comparing the correlation contours around the reference plane between $\rho_{[P,E^{\mathrm{ref}}]}$ in figure 13 and $\rho_{[-\langle u'v'\rangle, E^{\mathrm{ref}}]}$ in figure 14, the TKE is strongly correlated with the local Reynolds shear stress, whereas relatively decorrelated with TPR. The difference between the above two correlation contour must be due to the time-fluctuating mean shear. If a time- and plane-averaged mean flow was used the plane-averaged mean shear would then show no fluctuations in time and the correlation contours $\rho_{[P,E^{\mathrm{ref}}]}$ in figure 13 and $\rho_{[-\langle u'v'\rangle, E^{\mathrm{ref}}]}$ in figure 14 would be identical. The dynamics of the plane-average mean shear is therefore indispensable for the dynamics of TPR.

### 4.3. *Interplay between the Reynolds shear stress and the mean shear: a mechanistic model*

To reveal the dynamics of the plane-average mean shear and its relation with the place-average Reynolds shear stress, we plot in figure 15 the correlation between the Reynolds shear stress at the reference plane $y^{\mathrm{ref}} = 0.3H$ and the mean shear elsewhere (as already mentioned, the results for $y^{\mathrm{ref}} = 0.3H$ are indicative of any $y^{\mathrm{ref}}$ between 0.2 and 0.4). Very similar, if not near-identical, correlation maps (not shown here for brevity) are obtained for the correlation between TKE at the reference plane $y^{\mathrm{ref}} = 0.3H$ and the mean shear elsewhere. Around the reference plane, there exists a region of anti-correlation between plane-average Reynolds shear stress and mean shear with a spread of time lags. On the other hand, the mean shear in the near-wall region shows a positive correlation with the plane-average reference Reynolds shear stress in the near-equilibrium region. High/low TKE or Reynolds shear stress in the near-equilibrium region are followed with some time lag by low/high mean shear in the same region and by high/low mean shear fluctuations in the near-wall region. The anti-correlation of $\rho_{[dU/dy, -\langle u'v'\rangle^{\mathrm{ref}}]}$ in the near-equilibrium region in figure 15 resolves the discrepancy between anti-correlation in the contours of $\rho_{[P,E^{\mathrm{ref}}]}$ with time lag and $\rho_{[-\langle u'v'\rangle, E^{\mathrm{ref}}]}$.

The above observations may be interpreted by the following mechanistic model. Around the near-equilibrium region, when strong ejections and/or sweeps occur, high streamwise momentum in the outer region is transported towards the wall by sweeps and low streamwise momentum in the inner region is transported away from the wall by ejections, resulting in a local flattening of the mean velocity profile and reduction of the mean shear $\mathrm{d}U(y,t)/\mathrm{d}y$. Therefore, in the near-equilibrium region where viscosity plays little role, high values of $-\langle u'v'\rangle$, and therefore also TKE, precede low values of $\mathrm{d}U/\mathrm{d}y$ as well as resulting reduced values of TPR around the same $x$-$z$ plane. When high momentum in the outer region is transported to the near-wall region by sweeps, the overall near-wall momentum increases while the no-slip boundary condition at the wall is unaltered. As a result, the mean shear close to the wall becomes elevated, thereby explaining our observation of a positive correlation with positive time lag between $-\langle u'v'\rangle$ in the near-equilibrium region and $\mathrm{d}U/\mathrm{d}y$ in the near-wall region. Since both the near-wall Reynolds shear stress and the near-wall mean

shear are positively correlated with reference TKE in the near-equilibrium region with time lag, the near-wall TPR is also positively correlated with TKE in the near-equilibrium region as in figure 13. This mechanistic model therefore explains how TKE can precede TPR even though volume-average TPR obviously precedes, albeit slightly, TKE.

## 5. Conclusion

Dynamical interactions between turbulent energetics, specifically TKE (turbulent kinetic energy), TDR (turbulent dissipation rate) and TPR (turbulence production rate), have been studied in FD TCF using temporal correlations at Reynolds numbers up to $Re_\tau \simeq 2000$. By using a minimal computational domain capable of capturing the outer large-scale structures (Hwang & Cossu 2010), volume- and plane-averaged statistics fluctuate in time. For example, plane-averaged fields fluctuate in time, though of course less than fluctuating fields obtained by a Reynolds decomposition and therefore fluctuating around respective plane-averaged fields.

The volume-averaged TKE is found to be correlated with TDR at a later time (i.e. time lag) as in periodic/homogeneous turbulence (Goto & Vassilicos 2015) where this time lag was recognised as resulting from the turbulence energy cascade. The volume-averaged TPR is correlated with TKE at a later time simply because TPR is an energy input rate.

Moving to plane-averaged TKE, TDR and TPR at various wall-normal locations, correlations between plane-averaged TKE and TDR at the same plane reveal almost zero time lag/lead throughout the channel (as in Apostolidis *et al.* (2022)). The volume-averaged time lag between TKE and TDR must therefore result from non-local processes in the wall-normal direction.

Non-local correlations are then investigated with 2-time 2-plane correlations, i.e. correlations between plane-averaged TKE at a reference plane in the outer near-equilibrium region (where a local minimum in the 2-time 1-plane correlation is found between TKE and TDR) and plane-averaged TDR at another plane. Positive correlations between reference-plane TKE and core-region TDR have been revealed with positive time lags $\delta\tau$ and wall-distance lags $\delta y$ related by $\delta y/\delta\tau \approx u_\tau$ for all Reynolds numbers. There is, therefore, a correlation path from TKE at the outer near-equilibrium region to TDR in the core which is reminiscent of the momentum transport path by ejections (Flores & Jiménez 2010).

Another path of positive correlation between reference-plane TKE and near-wall region TDR has also been found with correlation velocities $\delta y/\delta\tau$ significantly smaller than $u_\tau$ and less well-defined. The path towards the near-wall region shows an increasing spread of time lags with increasing Reynolds number, as also, in fact, observed in the correlation between volume-averaged TKE and TDR. This is a mechanism by which turbulence in the outer part of the near equilibrium layer influences/controls near-wall TKE, TDR and TPR in a way that involves elevation of production/dissipation throughout the overlap and buffer layers. This mechanism is very different from the superposition and modulation effect described in Hutchins & Marusic (2007*b*) but is reminiscent of a similar effect seen by Doohan *et al.* (2022) at much lower Reynolds number.

A plane-local anti-correlation also exists between TKE and TDR in the same plane within the near-equilibrium region with time lag (from TKE to TDR). This anti-correlation signifies high/low TKE preceding low/high TDR around the reference plane. If the principal mechanism of depletion of local TKE occurs along the two spatio-temporal paths identified in the two preceding paragraphs so that high TDR follows high TKE along these paths, little amounts of TKE will be left on the reference plane thereby leading to relatively low TDR on that plane at later times.

Taking a reference plane near the wall rather than in the outer part of the near-equilibrium

region leads to significant instantaneous correlations between near-wall TKE and core-region TDR as well as near-wall TDR and core-region TDR. This observation points to an additional effect which may be that near-wall and core-region TDR are both controlled in a synchronised way by large energy-containing structures with sizes comparable to the half-channel height.

The relevance of ejections/sweeps to TKE transport has been studied by calculating plane-averaged TKE conditionally on ejections/sweeps. Ejection-based TKE correlates with TDR in a way similar to the unconditional TKE both in terms of the correlation velocity and levels of correlations, whereas the sweep-based TKE is significantly less correlated with TDR. It is hypothesised that the correlation is higher when conditioning plane-averaged TKE on ejections rather than sweeps along both paths towards the core and towards the wall because ejections have higher absolute values of Reynolds shear stress and are therefore better organised than sweeps.

While the volume-averaged TPR evidently precedes TKE, 2-time 2-plane correlations reveal that high/low reference-plane-average TKE precedes high/low plane-average TPR in both the core and near-wall regions when taking the reference plane in the outer near-equilibrium region. In this reference plane, plane-averaged TKE and plane-averaged TPR are anti-correlated with positive time lag from high/low TKE to low/high TPR.

We have explained these TPR observations with a mechanistic model. High instantaneous Reynolds shear stress flattens the local mean flow profile (reduces the local mean shear) in the near-equilibrium region as ejections and sweeps mix high streamwise momentum above with low streamwise momentum below the reference plane. It then strengthens the mean shear in the near-wall region as high streamwise momentum is brought close to the wall where viscosity kicks in.

**Funding.** This work is supported by the European Office of Aerospace Research and Development (EOARD) (FA8655-21-1-7016; Program Manager: Dr D. Smith).

**Acknowledgements.** This work is granted access to the HPC resources of IDRIS under the allocation 2022-021741 made by GENCI (Grand Equipement National de Calcul Intensif).

**Declaration of interests.** The authors report no conflict of interest.

## REFERENCES

Apostolidis, A., Laval, J.-P. & Vassilicos, J.C. 2022 Scalings of turbulence dissipation in space and time for turbulent channel flow. *J. Fluid Mech.* **946**, A41.

Bewley, T. 2014 *Numerical Renaissance: Simulation, Optimization, and Control*. Renaissance Press.

Cheng, C., Shyy, W. & Fu, L. 2022 Streamwise inclination angle of wall-attached eddies in turbulent channel flows. *J. Fluid Mech.* **946**, A49.

Ciola, N., De Palma, P., Robinet, J.-C. & Cherubini, S. 2023 Nonlinear optimal perturbation of turbulent channel flow as a precursor of extreme events. *J. Fluid Mech.* **970**, A6.

Doohan, P., Bengana, Y., Yang, Q., Willis, A. P. & Hwang, Y. 2022 The state space and travelling-wave solutions in two-scale wall-bounded turbulence. *J. Fluid Mech.* **947**, A41.

Doohan, P., Willis, A. P. & Hwang, Y. 2019 Shear stress-driven flow: the state space of near-wall turbulence as $Re_\tau \to \infty$ . *J. Fluid Mech.* **874**, 606–638.

Doohan, P., Willis, A. P. & Hwang, Y. 2021 Minimal multi-scale dynamics of near-wall turbulence. *J. Fluid Mech.* **913**, A8.

Farano, M., Cherubini, S., Robinet, J.-C. & De Palma, P. 2017 Optimal bursts in turbulent channel flow. *J. Fluid Mech.* **817**, 35–60.

Flores, O. & Jiménez, J. 2010 Hierarchy of minimal flow units in the logarithmic layer. *Phys. Fluids* **22** (7), 071704.

Frisch, U. 1995 *Turbulence: The Legacy of A. N. Kolmogorov*. Cambridge University Press.

Goto, S. & Vassilicos, J.C. 2015 Energy dissipation and flux laws for unsteady turbulence. *Phys. Lett.* A **379** (16), 1144–1148.

Goto, S. & Vassilicos, J. C. 2016 Local equilibrium hypothesis and taylor's dissipation law. *Fluid Dyn. Res.* **48** (2), 021402.

Guala, M., Hommema, S. E. & Adrian, R. J. 2006 Large-scale and very-large-scale motions in turbulent pipe flow. *J. Fluid Mech.* **554**, 521–542.

Hamilton, J. M., Kim, J. & Waleffe, F. 1995 Regeneration mechanisms of near-wall turbulence structures. *J. Fluid Mech.* **287**, 317–348.

Hoyas, S. & Jiménez, J. 2006 Scaling of the velocity fluctuations in turbulent channels up to $Re_\tau = 2003$. *Phys. Fluids* **18** (1), 011702.

Hutchins, N. & Marusic, I. 2007*a* Evidence of very long meandering features in the logarithmic region of turbulent boundary layers. *J. Fluid Mech.* **579**, 1–28.

Hutchins, N. & Marusic, I. 2007*b* Large-scale influences in near-wall turbulence. *Phil. Trans. R. Soc. Lond.* A **365** (1852), 647–664.

Hwang, Y. & Bengana, Y. 2016 Self-sustaining process of minimal attached eddies in turbulent channel flow. *J. Fluid Mech.* **795**, 708–738.

Hwang, Y. & Cossu, C. 2010 Self-sustained process at large scales in turbulent channel flow. *Phys. Rev. Lett.* **105**, 044505.

Jiménez, J. & Moin, P. 1991 The minimal flow unit in near-wall turbulence. *J. Fluid Mech.* **225**, 213–240.

Jiménez, J. & Pinelli, A. 1999 The autonomous cycle of near-wall turbulence. *J. Fluid Mech.* **389**, 335–359.

Kim, J. & Moin, P. 1985 Application of a fractional-step method to incompressible Navier-Stokes equations. *J. Comp. Phys.* **59** (2), 308–323.

Kim, K. C. & Adrian, R. J. 1999 Very large-scale motion in the outer layer. *Phys. Fluids* **11** (2), 417–422.

Kline, S. J., Reynolds, W. C., Schraub, F. A. & Runstadler, P. W. 1967 The structure of turbulent boundary layers. *J. Fluid Mech.* **30** (4), 741–773.

Kwon, Y. S., Philip, J., de Silva, C. M., Hutchins, N. & Monty, J. P. 2014 The quiescent core of turbulent channel flow. *J. Fluid Mech.* **751**, 228–254.

Lee, M. & Moser, R. D. 2015 Direct numerical simulation of turbulent channel flow up to $Re_\tau \approx 5200$. *J. Fluid Mech.* **774**, 395–415.

Lozano-Durán, A. & Jiménez, J. 2014*a* Effect of the computational domain on direct simulations of turbulent channels up to $Re_\tau = 4200$. *Phys. Fluids* **26** (1), 011702.

Lozano-Durán, A. & Jiménez, J. 2014*b* Time-resolved evolution of coherent structures in turbulent channels: characterization of eddies and cascades. *J. Fluid Mech.* **759**, 432–471.

Lu, S. S. & Willmarth, W. W. 1973 Measurements of the structure of the Reynolds stress in a turbulent boundary layer. *J. Fluid Mech.* **60** (3), 481–511.

Marusic, I. & Heuer, W. D. C. 2007 Reynolds number invariance of the structure inclination angle in wall turbulence. *Phys. Rev. Lett.* **99**, 114504.

Pirozzoli, S. 2023 Searching for the log law in open channel flow. *J. Fluid Mech.* **971**, A15.

Sagaut, P. & Cambon, C. 2008 *Homogeneous Turbulence Dynamics*. Cambridge University Press.

Townsend, A. A. 1961 Equilibrium layers and wall turbulence. *J. Fluid Mech.* **11** (1), 97–120.

Vassilicos, J.C. & Laval, J.-P. 2024 Scale-by-scale non-equilibrium in turbulent flows. In *Coarse Graining Turbulence: Modeling and Data-Driven Approaches and their Applications* (ed. F.F. Grinstein, F.S. Pereira & M. Germano). Cambridge University Press.

Vassilicos, J. C. 2015 Dissipation in turbulent flows. *Annu. Rev. Fluid Mech.* **47** (1), 95–114.

Waleffe, F. 1997 On a self-sustaining process in shear flows. *Phys. Fluids* **9** (4), 883–900.

Wallace, J. M., Eckelmann, H. & Brodkey, R. S. 1972 The wall region in turbulent shear flow. *J. Fluid Mech.* **54** (1), 39–48.

Willmarth, W. W. & Lu, S. S. 1972 Structure of the Reynolds stress near the wall. *J. Fluid Mech.* **55** (1), 65–92.

Yao, J., Chen, X. & Hussain, F. 2022 Direct numerical simulation of turbulent open channel flows at moderately high Reynolds numbers. *J. Fluid Mech.* **953**, A19.